

NASA TECHNICAL  
REPORT



NASA TR R-231

e.1

NASA TR R-231

0068514



THE ELECTROMAGNETIC TORQUES  
ON SPHERICAL EARTH SATELLITES  
IN A RAREFIED PARTIALLY  
IONIZED ATMOSPHERE

*by Frank Hohl*

*Langley Research Center*

*Langley Station, Hampton, Va.*



TECH LIBRARY KAFB, NM



0068514

THE ELECTROMAGNETIC TORQUES ON SPHERICAL EARTH SATELLITES  
IN A RAREFIED PARTIALLY IONIZED ATMOSPHERE

By Frank Hohl

Langley Research Center  
Langley Station, Hampton, Va.

NATIONAL AERONAUTICS AND SPACE ADMINISTRATION

---

For sale by the Clearinghouse for Federal Scientific and Technical Information  
Springfield, Virginia 22151 - Price \$3.00

# THE ELECTROMAGNETIC TORQUES ON SPHERICAL EARTH SATELLITES

## IN A RAREFIED PARTIALLY IONIZED ATMOSPHERE

By Frank Hohl  
Langley Research Center

### SUMMARY

A theoretical investigation has been made of the torques acting, as a result of electromagnetic interaction, on spherical conducting earth satellites. The analysis has been applied to the 41-meter-diameter satellite Echo II (1964 4A), which is in a near polar circular orbit. The calculations have yielded quantitative values for the accelerating and the decelerating torques. A probable explanation of the nearly constant spin rate of Echo II for a long period of time is that the eddy-current torque and the induction torque were in balance. Other torques are shown to be negligible in comparison with these two.

### INTRODUCTION

For a number of scientific experiments aboard artificial earth satellites, a knowledge of the satellite motion about its center of mass is required. The determination of the satellite motion is a complicated problem and many factors must be accounted for. Especially, the torques acting on the satellite must be known. It is also of interest to calculate the torques on a satellite to determine whether these torques are large enough to explain the fluctuation in the spin rate observed for some satellites - for example, the change of the spin rate of Sputnik I (1957 Alpha 2) reported in reference 1. The present paper reports a theoretical investigation of the torques acting on a spherical artificial earth satellite as a result of electromagnetic interaction with the ionized atmosphere and the earth's magnetic field. Apparently, some of the sources of torque have not been considered heretofore. In the course of the calculations, the currents flowing in the satellite hull are also determined. A knowledge of these currents may be desirable since they can influence certain scientific experiments aboard the satellite.

The present theory is applied to the 41-meter-diameter satellite Echo II (1964 4A). Calculation of and numerical results for the various torques acting on this satellite are presented. One peculiar aspect of Echo II is that the period of rotation of this satellite remained very nearly constant at about 100 seconds for a period of 280 days after launch. However, it is well known that the spin rate of the satellite as it spins in the earth's magnetic field

should be reduced by eddy-current damping with a time constant of only a few months. Thus, one is forced to look for accelerating torques to explain the nearly constant spin rate of Echo II. The initial spin-up of the satellite cannot be attributed to the torques calculated in this report. It is thought to be due to escaping gas from a probable rent in the satellite during and shortly after inflation.

The information on the construction and the spin rate of Echo II was obtained from an unpublished post launch account and analysis of the performance of Echo II prepared by the Goddard Space Flight Center.

## SYMBOLS

The mksAK system of units is used herein.

A	area
B	magnetic induction
e	charge on proton
$\hat{i}, \hat{j}, \hat{k}$	unit vector in x-, y-, and z-direction, respectively
i	electric current
j	electric current density
J	moment of inertia
k	Boltzmann constant
m	mass of particle
M	magnetic dipole moment
n	number density
P	power
Q	charge on satellite
$r, \theta, \psi$	spherical coordinates
R	resistance
S	surface resistivity
t	time
T	torque or temperature

$$U = \frac{e\phi}{kT}$$

V	velocity
x,y,z	Cartesian coordinates
X,Y,Z	axes
$\alpha$	angle defined by equation (3)
$\beta$	satellite colatitude
$\gamma$	current flux function
$\delta$	change in effective satellite radius defined by equation (9)
$\epsilon$	angle defined in figure 10
$\epsilon_1$	quantity defined by equation (11)
$\epsilon_0$	free space dielectric constant
$\epsilon_p$	quantity defined by equation (61)
$\epsilon'_p$	quantity defined by equation (63)
$\epsilon\phi$	quantity defined by equation (7)
$\zeta$	radial distance from center of satellite in Debye lengths
$\eta$	angle between satellite spin axis and magnetic field
$\lambda_D$	Debye length, $\left(\frac{kT\epsilon_0}{n_0e^2}\right)^{1/2}$
$\mu_0$	permeability of free space
$\nu$	convergence parameter defined by equation (50)
$\rho$	mass density
$\sigma$	surface charge density
$\tau$	inclination of current loop to XY-plane (see fig. 13)
$\phi$	electric potential
$\phi_{eq}$	satellite potential on a circumference where $(\vec{V}_s \times \vec{B}) \cdot \vec{r}_s = 0$

$\Phi$  magnetic flux  
 $\omega$  angular velocity

Subscripts:

a ambient  
e electron  
eff effective  
E earth  
i ion  
m summation index  
n normal component or summation index  
p photoemission  
s satellite  
x,y,z x,y, and z components  
 $\theta, \psi$   $\theta$  and  $\psi$  components

Mathematical notation:

$\rightarrow$  vector  
 $\hat{\phantom{x}}$  unit vector  
 $\langle \phantom{x} \rangle$  average over one earth orbit  
 $||$  absolute value

## SATELLITE ENVIRONMENT AND CONSTRUCTION OF ECHO II

Echo II (1964 4A) is at an average altitude of about 1200 km and is in a near circular polar earth orbit. Table I shows some of the pertinent parameters of the atmosphere for an altitude of 1200 kilometers. Atmospheric density, ion density, and temperature have been taken from Hanson (refs. 2 and 3) and Johnson (refs. 4 and 5). It is difficult to assign a definite temperature to the electrons and ions at the altitude of interest for the present calculations. Satellite data indicate that the temperature and density at high altitudes vary considerably with the 11-year solar cycle and also with the time of day. Since the results are to be compared with satellite data obtained near the minimum of the 11-year solar cycle, an ion temperature of  $1000^{\circ}$  K has been chosen. There

is evidence that the electron temperature is higher than the neutral gas temperature (refs. 3, 6, and 7). For this reason an electron temperature of  $1600^{\circ}$  K was used in the calculations.

Assumptions underlying the present investigation are that the satellite consists of a conducting nonferromagnetic spherical shell and that the satellite dimensions are large compared with a Debye length. By using the equations given by Spitzer (ref. 8) to determine the collision times for ions and electrons, the mean free paths for ions and electrons at an altitude of 1200 kilometers are shown in table I to be much larger than the satellite dimensions. Also, the number of revolutions about the magnetic field lines between collisions is large for both electrons and ions. Thus, the assumptions that there are no collisions and that the charged particles move along the magnetic field lines are justified. Another assumption is that the ions are singly ionized so that  $n_{i,a} = n_{e,a}$ . Experimental results by Bourdeau, Whipple, Donley, and Bauer (ref. 9) obtained from the Explorer VIII (1960 Xi 1) satellite support the assumption used herein that the electrons and the ions have Maxwellian velocity distributions.

Since a satellite cannot sustain a net current flow to or from the ionized atmosphere, the net flux of ions to the satellite must equal the electron flux. Since the thermal velocity of the electrons is much greater than that of the ions, the satellite will acquire a negative potential. If there is considerable photoemission, however, the satellite may acquire a positive potential. The method for calculating the ion and electron accretion by the satellite is similar to the method described by Hohl and Wood in reference 10.

Some of the parameters pertaining to Echo II are presented in table I. Echo II is a spherical shell of aluminum foil  $4.6 \times 10^{-6}$  meter thick bonded to both sides of Mylar polyester film  $8.9 \times 10^{-6}$  meter thick. There is no electrical continuity between the parts of the inner aluminum layer. By using the thickness of the outside aluminum layer of the satellite and the resistivity of aluminum at  $313^{\circ}$  K ( $3.1 \times 10^{-8}$  ohm-meter), the surface resistivity  $S$  is found to be  $6.7 \times 10^{-3}$  ohm.

The radius of Echo II is 20.5 meters and the mass of the satellite is 252.9 kilograms. The satellite rotates at a rate of about 0.063 radian per second. Data received from two beacons located  $180^{\circ}$  apart on the equator of Echo II indicate that the spin axis of the satellite is relatively fixed with respect to both space and the satellite. Evaluation of the data at the Goddard Space Flight Center also indicates that the spin axis is roughly parallel to the earth's magnetic dipole axis. With respect to the satellite, the spin axis is roughly normal to a plane which contains the line connecting the two beacons at the satellite equator. Thus, it is not determined whether the satellite spin axis points through the satellite pole caps, or lies in a plane containing the satellite equator, or lies anywhere between these two extremes.

## QUALITATIVE DESCRIPTION OF ELECTROMAGNETIC TORQUES

For the purpose of calculating the electromagnetic torques, the earth's magnetic field can be approximated by a dipole field. However, over the dimensions of a satellite the earth's magnetic field can be taken to be plane parallel in a direction determined by the direction of the earth's dipole field. The approximation of the earth's magnetic field by a dipole field can be used until effects of the solar wind destroy the dipole field. The effects of the solar wind are predominant at altitudes over about 9 earth radii. Thus, the dipole approximation should be valid out to several earth radii.

The electromagnetic torques acting on a satellite can be divided into two types. Torques of the first type result from the interaction of the metallic satellite hull with the earth's magnetic field. The relative motion of the satellite with respect to the earth's magnetic field may induce currents in the satellite hull; these currents can then interact with the earth's magnetic field to produce torques. Also, as the satellite passes across lines of force of the earth's magnetic field, a polarization of the satellite occurs. This polarization results in a nonuniform surface charge. If the satellite now rotates about its spin axis, the surface charge will keep its orientation with respect to the magnetic field and the satellite velocity vector and thus constitute a motion of electric charge relative to the conducting shell. The Joule heat dissipated by the current can be shown to come from the energy of rotation of the satellite. Thus, the first type of torque represents a damping torque acting on the satellite and would be present even if the satellite were moving in a nonionized atmosphere.

Torques of the second type result from the interaction of the satellite with the ionized atmosphere in the presence of the earth's magnetic field. These torques are the Coulomb torque and the induction torque. The Coulomb torque is due to unsymmetrical accretion of electrons and ions. If the satellite velocity is parallel to the earth's magnetic field or if there is no magnetic field, the satellite is unpolarized and the satellite cross section for ion impingement is as shown in figure 1. As indicated, the negative charge on the satellite causes the cross section for ion impingement to be increased symmetrically so that no Coulomb torques are developed. If, however, the satellite moves across lines of force of the earth's magnetic field, it becomes polarized and the cross section for ion impingement is increased on the more negative side of the satellite and decreased on the more positive side, as shown in figure 2. The unsymmetrical impingement of ions produces a torque. As was indicated by Hohl and Wood in reference 10, the momentum transferred by the ions that are scattered but that do not impact the satellite is negligible compared with the momentum transferred by the ions that impact the satellite as a result of the increase in effective cross section due to the charge on the satellite. It should also be noted that electrons contribute a negligible amount to the Coulomb torque, since the electrons impinge on the satellite from two sides along the magnetic field lines and the electron mass is much smaller than the ion mass.

The induction torque is the result of currents flowing in the satellite hull due to preferred accretion of electrons or ions on certain portions of the satellite surface. The induction torque is illustrated in figure 3. Ions impinge primarily on the front portion of the satellite, being concentrated somewhat on the more negative side of the satellite because of the increased cross section for ion interception. Electrons moving along the magnetic field lines impinge on the satellite principally on the side which is more positive. Qualitatively, the current is then as indicated in figure 3; in general, the resulting  $\vec{j} \times \vec{B}$  force does not pass through the center of the satellite and therefore it exerts a torque on the satellite. The energy put into rotation is taken from the kinetic energy associated with the satellite motion around the earth.

A nonelectrodynamic torque of interest is the aerodynamic torque due to the satellite spin. It is estimated herein in order to be compared with the other torques. In the calculation done in this report the satellite spin vector is pointing in the negative z-direction shown in figures 4 and 5.

#### SATELLITE POTENTIAL

In the absence of photoemission, an artificial earth satellite will acquire a net negative charge. The reason for the acquisition of the negative charge is that for an uncharged body moving at satellite velocity the rate of accretion of electrons is much greater than that of ions because the thermal velocity of the electrons is much higher than the velocity of the satellite or the thermal velocity of the ions. To keep the rate of electron accretion equal to that of ion accretion, the satellite will acquire a negative potential.

The equilibrium potential of the satellite is obtained by setting the sum of the electron current and the ion current to the satellite equal to zero - that is,

$$i_i + i_e = 0 \quad (1)$$

It is assumed that upon striking the satellite surface the ions become neutralized and either stick to the surface or are reflected or reemitted as neutral particles.

Experimental results of Hagstrum (refs. 11, 12, and 13) show that ions striking a metal surface will be neutralized by Auger charge exchange with an efficiency of nearly 100 percent. The experiments by Hagstrum also indicate that when the ions strike the metal surface some secondary electrons are produced. In the calculations that follow, these secondary electrons are neglected.

To determine the ion and the electron currents to the satellite, it is necessary to specify the orientations of the magnetic field, the satellite velocity vector, and the coordinate system to be used. This information is

contained in figure 4. The earth coordinate system is fixed with its origin at the earth's center. The satellite coordinate system has its origin at the center of the spherical satellite and the  $Z_S$  and  $X_S$  axes remain always parallel to the  $Z_E$  and  $X_E$  axes, respectively. Since the satellite is taken to be in a circular polar earth orbit at an altitude of 1200 kilometers, the earth's dipole field in the satellite coordinate system, as determined from the information in reference 14, is

$$\vec{B} = B_a \left[ -\hat{i} \beta \cos \beta \sin \beta + \hat{k} (1 - \beta \cos^2 \beta) \right] \quad (2)$$

with  $B_a = 1.9 \times 10^{-5}$  weber per square meter. The angle  $\alpha$  shown in figure 4 is given by

$$\tan \alpha = -\frac{\beta \cos \beta \sin \beta}{1 - \beta \cos^2 \beta} \quad (3)$$

The conditions for Echo II are such that the inequalities  $V_e \gg V_s$  and  $V_s \gg V_i$  can be assumed to hold. In reference 15, the second inequality is shown to result in an error in ion acquisition rate of only 4 percent on the front and 4 percent on the rear of the satellite at an altitude of 1200 kilometers. The kinetic-theory differential expression for the flux of particles along the magnetic field lines in one direction (with velocities along the field lines between  $V$  and  $V + dV$ ) is

$$dj_e = -en_a \left( \frac{m_e}{2\pi kT} \right)^{1/2} V \exp\left( \frac{-m_e V^2}{2kT} \right) dV \quad (4)$$

To obtain the electron current density to the satellite, equation (4) must be integrated between the kinetic energy limits  $-e\phi_s$  for  $\phi_s < 0$  and  $\infty$  and between the limits 0 and  $\infty$  for  $\phi_s \geq 0$ .

The electrons reach the satellite mainly along the magnetic field lines. When referred to the satellite orientation shown in figure 5, the electron current density to the spherical surface is

$$j_e = -en_a \left( \frac{kT}{2\pi m_e} \right)^{1/2} |\sin \theta \cos \psi \sin \alpha + \cos \alpha \cos \theta| \exp\left( \frac{e\phi_s \epsilon \phi}{kT} \right) \quad (5)$$

where the trigonometric factor comes from the dot product of the unit vectors  $\hat{r}$  and  $\hat{B}$  and where

$$\phi_s = \phi_{eq} + (\vec{V}_s \times \vec{B}) \cdot \vec{r}_s$$

$$\phi_s = \phi_{eq} + 2V_s B_a r_s \cos \beta \sin \theta \sin \psi \quad (6)$$

and

$$\left. \begin{aligned} \epsilon_\phi &= 1 & (\phi_s < 0) \\ \epsilon_\phi &= 0 & (\phi_s \geq 0) \end{aligned} \right\} \quad (7)$$

In equation (6) the ohmic potential drop has been neglected in comparison with the induced potential gradient. That the neglect of the ohmic drop is valid is seen in a subsequent section when the currents flowing in the satellite hull have been determined.

The symbol  $\epsilon_\phi$  is introduced to limit the maximum electron current that can be intercepted by the surface to that for which  $\phi_s = 0$ . Increasing the potential  $\phi_s$  above zero will not appreciably increase the electron current. The general behavior of the electron current as given by equation (5) has been experimentally verified by Bourdeau, Donley, Serbu, and Whipple (ref. 16) except that they found a small reduction in electron current on the back side of the satellite which is probably due to a negative charge in the wake.

The ion current to the satellite is obtained from the rate at which the ions are swept up by the effective satellite cross section for ion interception and is given by

$$i_i = n_a e V_s A_{eff} \quad (8)$$

Ion current measurements on the Explorer VIII satellite at an altitude of 1000 kilometers are in good agreement with the assumption that the ions are incident only on the front surface of the satellite irrespective of the orientation of the earth's magnetic field.

The effective cross-sectional area for ion interception  $A_{eff}$  and the equilibrium potential  $\phi_{eq}$  can be determined by successive approximations as follows: With a tentative value for  $\phi_{eq}$ , the potential distribution around the satellite is determined. Then, the ion trajectories are calculated to give  $A_{eff}$ . These values of  $\phi_{eq}$  and  $A_{eff}$  are then used to determine whether the net current to the satellite is zero. However, the result given by Jastrow and Pearse (ref. 17) for the sheath thickness approximates the results that are obtained when the actual trajectories are calculated; that is, any ion which approaches the satellite with an impact parameter greater than

$$r_{eff} \approx r_s - \frac{|\phi_s|}{\phi_s} \sqrt{\frac{2e|\phi_s|}{kT}} \lambda_D = r_s + \delta \quad (9)$$

will not be intercepted by the satellite, whereas any ion which approaches the satellite with an impact parameter less than  $r_s + \delta$  will be intercepted. The effective radius of the satellite for ion interception is then approximated by equation (9).

Comparisons of the effective satellite radius as obtained from equation (9) and as obtained by computing ion trajectories are made in the appendix.

When referred to the coordinate system shown in figure 5, the ion current density to the satellite becomes

$$j_i = en_a V_s \left( \frac{r_{\text{eff}}}{r_s} \right)^2 (\cos \beta \sin \theta \cos \psi - \sin \beta \cos \theta) \epsilon_i \quad (10)$$

where

$$\left. \begin{array}{l} \epsilon_i = 1 \\ \epsilon_i = 0 \end{array} \right\} \begin{array}{l} \left( \begin{array}{l} \cos \beta \sin \theta \cos \psi \\ - \sin \beta \cos \theta \end{array} \geq 0 \right) \\ \left( \begin{array}{l} \cos \beta \sin \theta \cos \psi \\ - \sin \beta \cos \theta \end{array} < 0 \right) \end{array} \quad (11)$$

The equilibrium potential is determined from

$$\int_A j_e dA + \int_A j_i dA = 0 \quad (12)$$

where the integration is over the spherical satellite surface.

Figure 6 gives the equilibrium potential of a spherical satellite as a function of its radius (conditions are the same as those for Echo II) for a typical value of  $\vec{V}_s \times \vec{B}$ . The equilibrium potential is a function of  $V_s$ ,  $B$ , and  $r_s$  and decreases nearly linearly with increasing  $r_s$ . If equation (12) is written explicitly, it can be deduced that the equilibrium potential will decrease nearly linearly with increasing  $B$ .

In figure 7(a) the equilibrium potential is given as a function of colatitude for Echo II. The results of figure 7(a) indicate that for Echo II the equilibrium potential can be approximated by

$$\phi_{\text{eq}} = -0.2 - 4.36 |\cos \beta| \quad (13)$$

and, therefore, the satellite potential can be approximated by

$$\phi_s = -0.2 - 4.36 |\cos \beta| + 5.67 \cos \beta \sin \theta \quad (14)$$

Experimental results show that the effect of photoelectric emission is generally not negligible; therefore, photoemission should be included in the calculations. Chang and Smith (ref. 18) and Brundin (ref. 19) have calculated the photoelectric emission from a satellite by considering the radiation incident on the satellite and by using an appropriate absorption coefficient and work function. However, since experimental measurements of photoemission are available, the measured currents can be used to determine the effects of photoemission on the equilibrium potential and on the torques. Considering the results obtained by Bourdeau, Donley, Serbu, and Whipple (ref. 16) from Explorer VIII data, a reasonable value for the photoelectric current is  $5 \times 10^{-5}$  ampere per square meter. If the satellite is in sunlight, the equilibrium potential is obtained from

$$\int_A j_e dA + \int_A j_i dA + 5 \times 10^{-5} \pi r_s^2 = 0 \quad (15)$$

The resulting equilibrium potential as a function of colatitude is given in figure 7(b). The equilibrium potential with photoemission can then be written as

$$\phi_{eq} = -0.165 - 1.688 |\cos \beta| \quad (16)$$

If the satellite surface has a positive potential, the photoelectric emission current will be reduced. The dependence of the photoelectric emission current on the positive satellite potential has been neglected in the foregoing calculations. Since most of the satellite surface is always negative, the error introduced should not be large.

#### RETARDING TORQUE DUE TO SURFACE CHARGE

The induced potential gradient on the satellite is  $\vec{V}_s \times \vec{B}$ . Thus, there exists a potential difference across the satellite which equals the induced potential difference minus the ohmic voltage drop; this ohmic voltage drop, however, is negligible. Therefore, the potential difference across the satellite is given by

$$\phi = 4r_s V_s B_a \cos \beta \quad (17)$$

The maximum potential induced across Echo II (over the earth's poles) is found to be about 11 volts. The potential difference polarizes the satellite by producing a surface charge. As the satellite rotates, the orientation of the surface charge with respect to the earth's magnetic field and the satellite velocity will remain the same. Thus, there is an electric current over the satellite surface. The resulting Joule losses tend to reduce the rate of rotation of the satellite.

To obtain the surface charge, the potential distribution through the sheath could be calculated numerically. However, if it is assumed that the satellite is in vacuum, the variation of potential around the satellite is given by a solution (ref. 20) of Laplace's equation - namely,

$$\phi = \frac{\phi_{eq} r_s}{r} - \frac{V_s B r_s^2}{r^2} \cos \theta \quad (18)$$

where the orientation of the satellite coordinate system has been so chosen that  $\vec{V}_s$  is along the Y-axis and  $\vec{B}$  is along the X-axis. Inasmuch as the surface charge density  $\sigma$  is equal to the normal component of the dielectric displacement at the surface,

$$\begin{aligned} \sigma &= -\epsilon_0 \left( \frac{\partial \phi}{\partial r} \right)_{r=r_s} \\ \sigma &= \epsilon_0 \frac{\phi_{eq}}{r_s} - 2\epsilon_0 V_s B \cos \theta \end{aligned} \quad (19)$$

To determine the maximum torque, the satellite is assumed to rotate about the Y-axis, because the resulting flow rate of surface charge is then a maximum. In the coordinate system in which the surface charge is at rest, the surface current density due to the satellite rotation is

$$\begin{aligned} \vec{j} &= \sigma (\vec{r}_s \times \vec{\omega}) \\ \vec{j} &= 2\epsilon_0 V_s B r_s \omega \cos \theta (\hat{i} \cos \theta - \hat{k} \sin \theta \cos \psi) \end{aligned} \quad (20)$$

The rate at which the current liberates Joule heat is

$$P = \int_A j^2_s dA = \frac{64}{15} \pi (\epsilon_0 V_s r_s^2 B \omega)^2 S \quad (21)$$

The energy source for the Joule heat is the kinetic energy of the rotating shell. Differentiating the equation of kinetic energy for the rotating

spherical shell gives

$$\frac{d}{dt} \left( \frac{1}{2} J \omega^2 \right) = \omega J \frac{d\omega}{dt} = -P \quad (22)$$

and thus the corresponding decelerating torque is

$$T = J \frac{d\omega}{dt} = -\frac{P}{\omega}$$

$$T = -\frac{64}{15} \pi S \omega \left( \epsilon_0 V_s r_s^2 B \right)^2 = -6 \times 10^{-20} \omega \text{ newton-meter} \quad (23)$$

In equation (23), the parameters pertaining to Echo II have been used. For any reasonable value of  $\omega$ , the decelerating torque is completely negligible in comparison with other torques that are considered herein.

#### RETARDING TORQUES DUE TO EDDY CURRENTS

It is well known that in the presence of a magnetic field the angular velocity of a conductor tends to be decreased (ref. 21). If the satellite rotates about an axis parallel to the magnetic field, no eddy currents are induced because of the rotation. If, however, the satellite rotates about an axis which has a component perpendicular to the magnetic field, eddy currents are induced in the conducting hull of the satellite. A number of papers have been written on the subject of eddy-current torques (for example, refs. 22, 23, and 24). Thus for Echo II only the torque for two specific orientations are considered.

The retarding torque due to the eddy currents in a uniformly conducting spherical shell has been shown by Halverson and Cohen (ref. 25) to be, when the spin axis is parallel to the Z-axis,

$$\vec{T} = -\frac{\pi \omega r_s^4 B^2}{9S^2 + \mu_0^2 \omega^2 r_s^2} \left[ \left( -\hat{i} 3S + \hat{j} \mu_0 \omega r_s \right) \sin 2\eta + \hat{k} 6S \sin^2 \eta \right] \quad (24)$$

For Echo II  $S \gg \mu_0 \omega r_s$  so that, if the satellite were uniformly conducting, the torque would be

$$\vec{T} = -\frac{\pi \omega r_s^4 B^2}{3S} \left( -\hat{i} \sin 2\eta + \hat{k} 2 \sin^2 \eta \right) \quad (25)$$

where  $\eta$  is the angle between the spin axis of the satellite and the magnetic field. Since the satellite spin axis is along the Z-axis for the present

problem, the angle  $\eta$  is equal to the angle  $\alpha$  indicated in figures 4 and 5. The satellite coordinate system shown in figures 4 and 5 is that used for most of the calculations. On substitution of equation (2) for  $B$  in equation (25) the torque becomes

$$\vec{T} = -\frac{\pi\omega r_s^4 B_a^2}{3S}(1 + 3 \cos^2\beta)(-\hat{i} \sin 2\alpha + \hat{k} 2 \sin^2\alpha) \quad (26)$$

The components of the eddy-current torque for the parameters of Echo II are shown in figure 8 as a function of  $\beta$ . Because of symmetry the torque is shown for only one-half orbit.

This eddy-current torque was calculated under the assumption that the satellite consists of a uniformly conducting spherical shell. However, Echo II is made up of 106 individual gores which are electrically connected only near the poles, as shown in figure 9. Thus, a better approximation to the torque can be obtained by assuming that the current paths are only along the gores.

To calculate the eddy-current torque for Echo II, the orientation of the satellite with respect to the spin axis must also be specified. Two cases of satellite orientation with respect to the spin axis are considered: case I - the satellite is spinning about an axis through its poles; case II - the satellite is spinning about an axis which lies in the plane of the satellite equator. The satellite orientation for case I is shown in figure 10. Note that the orientation of the coordinate system with respect to the earth remains as indicated in figures 4 and 5 and that  $B$  remains in the ZX-plane as indicated in figure 10. Consider the eddy currents flowing in circles (along the gores) through the poles. If it is assumed that the magnetic field due to the eddy currents can be neglected, the magnetic flux through a ring made up of two gores on opposite sides of the satellite becomes

$$\Phi = \pi r_s^2 B \sin \alpha \sin \psi$$

$$\Phi = \pi r_s^2 B \sin \alpha \sin \omega t \quad (27)$$

The electromotive force producing current in the ring is thus

$$\phi = -\frac{d\Phi}{dt} = -\omega\pi r_s^2 B \sin \alpha \cos \omega t \quad (28)$$

The resistance of the ring is

$$R = 2S \int_{\epsilon}^{\pi-\epsilon} \frac{d\theta}{\Delta\psi \sin \theta}$$

$$R = \frac{2S}{\Delta\psi} \log_e \left[ \frac{\tan\left(\frac{\pi - \epsilon}{2}\right)}{\tan\left(\frac{\epsilon}{2}\right)} \right] \quad (29)$$

where  $\epsilon$  is the angle indicated in figure 10 to the point where the gores are electrically connected to each other and  $\Delta\psi$  is the angle corresponding to the angular width of the gores.

The angle  $\epsilon$  where the gores are connected to the connecting ring is 0.03 radian. Using in equation (29) this value of  $\epsilon$  and  $6.7 \times 10^{-3}$  ohm for the surface resistivity  $S$  gives the value of the resistance  $R$  as 1.8 ohms. In this calculation, however, the resistance of the connecting ring and that of the connections where the connecting ring is ultrasonically welded to the gores were neglected. Measurements on the backup satellite for Echo II indicate that the average value of the resistance at each connection (not including the connections that were open circuits) was about 0.65 ohm. If this value is assumed to be applicable to the satellite that was launched, then the value of  $R$  to be used for the present calculations should be increased to 4.4 ohms.

The current flowing in a ring consisting of two gores is

$$i_\theta = \frac{\phi}{R} = -\frac{\pi}{R} r_s^2 B \omega \sin \alpha \cos \psi \quad (30)$$

The magnetic moment of the current is

$$\vec{M} = i\vec{A}$$

The torque on the ring can now be calculated from

$$\begin{aligned} \vec{T} &= \vec{M} \times \vec{B} \\ &= -\frac{\omega}{R} \pi^2 r_s^4 B^2 \sin \alpha \cos \psi (\hat{i} \sin \psi + \hat{j} \cos \psi) \times (\hat{i} \sin \alpha + \hat{k} \cos \alpha) \\ \vec{T} &= -\frac{\omega}{R} \pi^2 r_s^4 B^2 \sin \alpha \cos \psi (\hat{i} \cos \alpha \cos \psi - \hat{j} \cos \alpha \sin \psi - \hat{k} \sin \alpha \cos \psi) \end{aligned} \quad (31)$$

Averaging over  $\psi = \omega t$  and using  $B^2 = B_a^2 (1 + 3 \cos^2 \beta)$  gives

$$\vec{T} = -\frac{\omega}{4R} \pi^2 r_s^4 B_a^2 (1 + 3 \cos^2 \beta) (-\hat{i} \sin 2\alpha + \hat{k} 2 \sin^2 \alpha) \quad (32)$$

Since there are 53 such rings, the total torque on the satellite is

$$\vec{T} = -\frac{53\omega}{4R}\pi^2 r_s^4 B_a^2 (1 + 3 \cos^2 \beta) (-\hat{i} \sin 2\alpha + \hat{k} 2 \sin^2 \alpha) \quad (33)$$

The torque given by equation (33) would be the correct torque if all the gores were electrically connected to the connecting ring. However, electrical continuity measurements on the backup satellite for Echo II showed that about one-fourth of the connections between the gores and the connecting ring at each connecting ring represented open circuits (no continuity). One can therefore assume that about one-half of the gores were not connected either to the top or to the bottom connecting ring. The open circuits will very likely decrease the eddy-current torque by a factor of more than 2, since both ends of a gore must be connected for eddy current to flow. To obtain a better approximation for the eddy-current torque experienced by Echo II, the torque given by equation (33) is divided by 3. The factor of 3 was arrived at by the author after considering probable combinations of open circuits. The resulting components of the torque as a function of  $\beta$  are shown in figure 11. It can be seen that the torque curves for Echo II are the same as the curves for the uniformly conducting spherical shell except for a reduction in magnitude.

The orientation for case II is shown in figure 12. Consider the ring inclined at the angle  $\tau$  to the XY-plane. The flux through this ring is

$$\Phi = \pi r_s^2 B (\cos \alpha \cos \tau - \sin \alpha \sin \tau \cos \omega t) \quad (34)$$

where

$$\omega t = \psi$$

Thus, the potential induced in the ring is

$$\phi = -\frac{d\Phi}{dt} = -\omega B \pi r_s^2 \sin \alpha \sin \tau \sin \omega t \quad (35)$$

The current flowing along the gore (at  $\tau$ ) is

$$i = -\frac{\omega}{R} \pi r_s^2 B \sin \alpha \sin \tau \sin \omega t \quad (36)$$

Again, the torque on the ring is obtained from

$$\begin{aligned}
\vec{T} &= \vec{M} \times \vec{B} \\
&= -\frac{\omega_B^2 \pi^2 r_s^4}{R} \sin \alpha \sin \tau \sin \psi \left( -\hat{i} \sin \tau \cos \psi \right. \\
&\quad \left. - \hat{j} \sin \tau \sin \psi + \hat{k} \cos \tau \right) \times \left( \hat{i} \sin \alpha + \hat{k} \cos \alpha \right) \\
\vec{T} &= \frac{\omega_B^2 \pi^2 r_s^4}{R} \sin \alpha \sin \tau \sin \psi \left[ -\hat{i} \sin \tau \cos \alpha \sin \psi \right. \\
&\quad \left. + \hat{j} (\cos \tau \sin \alpha + \sin \tau \cos \alpha \cos \psi) + \hat{k} \sin \tau \sin \alpha \sin \psi \right] \quad (37)
\end{aligned}$$

Averaging over  $\psi = \omega t$  and using  $B^2 = B_a^2 (1 + 3 \cos^2 \beta)$  gives

$$\vec{T} = -\frac{\omega_B^2 \pi^2 r_s^4}{2R} B_a^2 (1 + 3 \cos^2 \beta) \left( -\hat{i} \sin^2 \tau \cos \alpha \sin \alpha + \hat{k} \sin^2 \tau \sin^2 \alpha \right) \quad (38)$$

To get the total torque the sum over  $\tau = n \Delta\psi$  is required - that is,

$$\vec{T} = -\frac{\omega_B^2 \pi^2 r_s^4}{4R} B_a^2 (1 + 3 \cos^2 \beta) \left( -\hat{i} \sin 2\alpha + \hat{k} 2 \sin^2 \alpha \right) \sum_{n=0}^{53} \sin^2(n \Delta\psi) \quad (39)$$

The resulting components of this torque as a function of  $\beta$  are indicated in figure 13, where equation (39) has been divided by the factor 3 to account for open circuits.

It should be noted that in its orbit around the earth the satellite will encounter a varying magnetic field. However, since  $\omega$  is much larger than the rate of revolution of the satellite around the earth, it can be assumed that the direction of the field does not change appreciably during a rotation of the satellite about its axis. The effect of the time varying earth's magnetic field with respect to the coordinate system fixed in the satellite can therefore be neglected. The problem of a satellite which remains stationary relative to the coordinate system moving with it in its orbit around the earth has been considered by Zonov (ref. 24).

#### COULOMB TORQUE

The Coulomb torque is due to unsymmetrical accretion of ions. The polarization of the satellite causes more ions to be intercepted by the more negative side of the satellite than by the more positive side. Thus an unsymmetrical transfer of momentum occurs which results in a torque on the satellite. The contribution to the torque from the ions that are deflected but do not strike

the satellite is negligible as indicated by Jastrow and Pearse (ref. 17) and by Hohl and Wood (ref. 10). To obtain the Coulomb torque the ion trajectories might first be calculated; this was done by Hohl and Wood in reference 10 for Explorer IX (1961 Delta 1). The maximum impact parameters for impingement obtained from these trajectories are in reasonably good agreement with the theory given by Jastrow and Pearse. Thus, even though the satellite potential is not spherically symmetric, the Jastrow-Pearse theory applied to a point of the satellite surface gives the approximate thickness of the sheath at that point. A comparison of sheath thickness as determined from calculations of ion trajectories with that given by the Jastrow and Pearse theory is given in the appendix.

If the Coulomb torque were found to be a considerable fraction of the torque required to balance the eddy-current torque, a more exact method would have to be used in calculating the Coulomb torque. However, since the Coulomb torque will be found negligible compared with some of the other torques, a 10- to 30-percent uncertainty in it will not affect any of the results. Thus, the effective satellite radius for ion interception can be sufficiently well approximated by the Jastrow and Pearse result (eq. (9)).

The calculation of the Coulomb torque is simplified if the satellite coordinate system shown in figure 14 is used. The magnetic field  $\vec{B}$  and the satellite velocity  $\vec{V}_s$  are then in the XY-plane and the satellite potential  $\phi_s$  is given by

$$\phi_s = \phi_{eq} - 2V_s B_a r_s \cos \beta \cos \theta' \quad (40)$$

If it is assumed that the ions transfer their momentum to the satellite at the point where they are intercepted by the sheath, the magnitude of the torque can be approximated as

$$\begin{aligned} T(\beta) &= 2m_i n_i V_s^2 \int_0^\pi \int_{r_s}^{r_s+\delta} r^2 \cos \theta' dr' d\theta' \\ &= \frac{2}{3} m_i n_i V_s^2 \int_0^\pi \left[ (r_s + \delta)^3 - r_s^3 \right] \cos \theta' d\theta' \\ T(\beta) &= \frac{2}{3} m_i n_i V_s^2 \int_0^\pi \left[ \left( r_s - \frac{|\phi_s|}{\phi_s} \sqrt{\frac{2\epsilon_0}{\eta_e e} |\phi_s|} \right)^3 - r_s^3 \right] \cos \theta' d\theta' \quad (41) \end{aligned}$$

Equation (41) gives the torque for the condition in which the ions that strike the satellite "stick" to the satellite surface. If the ions strike the satellite surface and are reemitted, the torque will be different. If the ions strike the surface and are reemitted as neutral particles, the contribution to the torque resulting from the neutralized ions recoiling from the front surface

of the satellite would have to be considered; that is, most of the ions which strike the satellite surface have been accelerated by the electric field of the satellite and, hence, if the ions are reflected as neutral particles, their final velocity after reflection will be much larger than their initial velocity. The radial component of the electric field of the satellite will accelerate the ions in such a manner that they cannot contribute to the torque. However, since the potential around the satellite is not completely radial, the neutralized ions recoiling from the front surface of the satellite with a velocity larger than their initial velocity would produce a torque. The computation of this torque is complicated because the ion trajectories must all be computed. An approximate method used to calculate the torque due to the recoiling neutralized ions yields results of the same order of magnitude as those obtained by use of equation (41) for the Coulomb torque. For the present calculation, only the torque due to the impingement, and not the reemission, of the ions is considered.

With reference to figure 4, the torque is found to be either parallel or anti-parallel to the radius vector from the center of the earth through the center of the satellite - that is,

$$\vec{T}(\beta) = -T(\beta) \left( \hat{i} \sin \beta + \hat{k} |\cos \beta| \right) \quad (42)$$

The components of the torque as calculated for Echo II by use of equations (41) and (42) are shown as a function of  $\beta$  in figure 15. Note that the torques are always referred to the coordinate system shown in figures 4 and 5.

#### INDUCTION TORQUE

The induction torque is by far the largest of the accelerating torques and is considerably more difficult to compute than any of the other torques. To determine the torque resulting from the unsymmetrical accretion of charge, the current distribution over the satellite surface must be found. The current distribution is calculated for a uniformly conducting spherical satellite and for Echo II where the spherical shell is made up of gores that are electrically connected together only near the poles.

To obtain the current distribution for a uniformly conducting spherical satellite, the coordinate system shown in figures 4 and 5 is used. By addition of equations (5) and (10) the current density to a point on the satellite surface without photoelectric emission is

$$j_i + j_e = en_a V_s \left( \frac{r_{eff}}{r_s} \right)^2 (\cos \beta \sin \theta \cos \psi - \sin \beta \cos \theta) \epsilon_i - en_a \left( \frac{kT}{2\pi m_e} \right)^{1/2} \left| \sin \theta \cos \psi \sin \alpha + \cos \alpha \cos \theta \right| \exp \left( \frac{e\phi_s \epsilon_i}{kT} \right) \quad (43)$$

If the increased satellite cross section for ion interception is neglected in the calculations of the induction torque, the resulting error is less than 1 percent. Using the approximate expression for the effective cross-sectional area given by equation (9) makes the error even smaller.

Let  $\vec{j}_s$  be the surface current density over the satellite surface. Then  $\vec{j}_s$  can be expressed as

$$\vec{j}_s = -\nabla\gamma \quad (44)$$

where  $\gamma$  is determined from

$$\nabla^2\gamma = \frac{1}{r_s^2 \sin^2\theta} \left[ \sin\theta \frac{\partial}{\partial\theta} \left( \sin\theta \frac{\partial\gamma}{\partial\theta} \right) + \frac{\partial^2\gamma}{\partial\psi^2} \right] = -(\mathbf{j}_i + \mathbf{j}_e) \quad (45)$$

In finite difference form equation (45) becomes

$$\begin{aligned} & \gamma_{n-1,m} \left[ \frac{\sin^2\theta_n}{(\Delta\theta)^2} - \frac{\sin\theta_n \cos\theta_n}{2\Delta\theta} \right] + \gamma_{n,m-1} \left( \frac{1}{\Delta\psi} \right)^2 + \gamma_{n+1,m} \left[ \frac{\sin^2\theta_n}{(\Delta\theta)^2} + \frac{\sin\theta_n \cos\theta_n}{2\Delta\theta} \right] \\ & + \gamma_{n,m+1} \left( \frac{1}{\Delta\psi} \right)^2 - 2\gamma_{n,m} \left[ \frac{\sin^2\theta_n}{(\Delta\theta)^2} + \left( \frac{1}{\Delta\psi} \right)^2 \right] = -r_s^2 \sin^2\theta_n (\mathbf{j}_i + \mathbf{j}_e) \end{aligned} \quad (46)$$

where  $\Delta\theta$  and  $\Delta\psi$  represent the separation of the mesh point used in the numerical solution. The values of subscript  $m$  are 1, 2, . . . ,  $M$  and those of subscript  $n$  are 1, 2, 3, . . . ,  $N$ . The mesh points are specified by

$$\psi_m = (m-1)\Delta\psi \quad \left( \Delta\psi = \frac{2\pi}{M} \right) \quad (47)$$

$$\theta_n = \left( n - \frac{1}{2} \right) \Delta\theta \quad \left( \Delta\theta = \frac{\pi}{N} \right) \quad (48)$$

The boundary conditions are

$$\left. \begin{aligned} \gamma_{N+1,m} &= \gamma_{N,m \pm \frac{M}{2}} & \gamma_{n,M+1} &= \gamma_{n,1} \\ \gamma_{0,m} &= \gamma_{1,m \pm \frac{M}{2}} & \gamma_{n,0} &= \gamma_{n,M} \end{aligned} \right\} \quad (49)$$

The equation actually used for the numerical solution on the IBM 7094 data processing system was of the form

$$\begin{aligned}
 \gamma_{n,m}^{(r+1)} = \gamma_{n,m}^{(r)} + \nu & \left( \frac{-1}{2 \left[ \frac{\sin^2 \theta_n}{(\Delta \theta)^2} + \left( \frac{1}{\Delta \psi} \right)^2 \right]} \left\{ r_s^2 \sin^2 \theta_n f(\theta_n, \psi_m) - \gamma_{n-1,m}^{(r+1)} \left[ \frac{\sin^2 \theta_n}{(\Delta \theta)^2} \right. \right. \right. \\
 & \left. \left. - \frac{\sin \theta_n \cos \theta_n}{2 \Delta \theta} \right] - \gamma_{n,m-1}^{(r+1)} \left( \frac{1}{\Delta \psi} \right)^2 - \gamma_{n+1,m}^{(r)} \left[ \frac{\sin^2 \theta_n}{(\Delta \theta)^2} + \frac{\sin \theta_n \cos \theta_n}{2 \Delta \theta} \right] \right. \\
 & \left. \left. - \gamma_{n,m+1}^{(r)} \left( \frac{1}{\Delta \psi} \right)^2 \right\} - \gamma_{n,m}^{(r)} \right) \quad (50)
 \end{aligned}$$

where  $f(\theta_n, \psi_m) = -(\mathbf{j}_e + \mathbf{j}_i)$  and  $\nu$  is a variable ( $1 < \nu < 2$ ) which was used to speed convergence and the magnitude of which was determined by the rate of convergence. The superscript (r) indicates the rth iteration. The torque due to the surface currents is determined from

$$\vec{T} = \int_0^{2\pi} \int_0^\pi \left[ \vec{r}_s \times (\vec{j}_s \times \vec{B}) \right] r_s^2 \sin \theta \, d\theta \, d\psi \quad (51)$$

or

$$\begin{aligned}
 T_x = r_s^3 B_a (1 + 3 \cos^2 \beta)^{1/2} & \int_0^{2\pi} \int_0^\pi \left[ j_\theta \cos \theta (\sin \theta \sin \alpha \right. \\
 & \left. + \cos \theta \cos \psi \cos \alpha - \sin \theta \sin^2 \psi \sin \alpha) \right. \\
 & \left. - j_\psi \sin \psi (\sin \theta \cos \psi \sin \alpha + \cos \theta \cos \alpha) \right] \sin \theta \, d\theta \, d\psi \quad (52)
 \end{aligned}$$

$$\begin{aligned}
 T_y = r_s^3 B_a (1 + 3 \cos^2 \beta)^{1/2} & \int_0^{2\pi} \int_0^\pi \left[ j_\theta \cos \theta \sin \psi (\cos \theta \cos \alpha \right. \\
 & \left. + \sin \theta \cos \psi \sin \alpha) + j_\psi \cos \psi (\cos \theta \cos \alpha \right. \\
 & \left. + \sin \theta \cos \psi \sin \alpha) \right] \sin \theta \, d\theta \, d\psi \quad (53)
 \end{aligned}$$

$$T_z = r_s^3 B_a (1 + \beta \cos^2 \beta)^{1/2} \int_0^{2\pi} \int_0^\pi \left[ j_\theta \sin \theta (\sin \theta \cos \psi \sin \alpha - \cos \theta \cos \alpha) \right] \sin \theta \, d\theta \, d\psi \quad (54)$$

The two components of  $\vec{j}_s$  are given by

$$j_\theta = \frac{\gamma_{n-1,m} - \gamma_{n+1,m}}{2 \Delta \theta r_s} = (j_\theta)_{n,m} \quad (55)$$

and

$$j_\psi = \frac{\gamma_{n,m-1} - \gamma_{n,m+1}}{2 \Delta \psi r_s \sin \theta} = (j_\psi)_{n,m} \quad (56)$$

By using the results of the numerical solutions for  $j_\theta$  and  $j_\psi$ , the components of  $\vec{T}$  are obtained from

$$T_x = r_s^3 B_a (1 + \beta \cos^2 \beta)^{1/2} \sum_n \sum_m \left[ (j_\theta)_{n,m} \cos \theta_n (\sin \theta_n \sin \alpha + \cos \theta_n \cos \psi_m \cos \alpha - \sin \theta_n \sin^2 \psi_n \sin \alpha) - (j_\psi)_{n,m} \sin \psi_m (\sin \theta_n \cos \psi_m \sin \alpha + \cos \theta_n \cos \alpha) \right] \sin \theta_n \Delta \theta \Delta \psi \quad (57)$$

$$T_y = r_s^3 B_a (1 + \beta \cos^2 \beta)^{1/2} \sum_n \sum_m \left[ (j_\theta)_{n,m} \cos \theta_n \sin \psi_m (\cos \theta_n \cos \alpha + \sin \theta_n \cos \psi_n \sin \alpha) + (j_\psi)_{n,m} (\cos \psi_m \cos \theta_n \cos \alpha + \sin \theta_n \cos \psi_m \sin \alpha) \right] \sin \theta_n \Delta \theta \Delta \psi \quad (58)$$

$$T_z = r_s^3 B_a (1 + \beta \cos^2 \beta)^{1/2} \sum_n \sum_m \left[ (j_\theta)_{n,m} \sin \theta_n (\sin \theta_n \cos \psi_m \sin \alpha - \cos \theta_n \cos \alpha) \right] \sin \theta_n \Delta \theta \Delta \psi \quad (59)$$

The induction torque for the uniformly conducting satellite without photo-emission as given by equations (57) and (59) is shown in figure 16. No

$T_y$  component is shown in figure 16, since the computed value of  $T_y$  was smaller than the error in the numerical computations.

If photoemission is included in the determination of the induction torque, then the orientation of the satellite orbit with respect to the earth-sun line must be specified. The induction torque with photoemission is calculated for two orientations. With reference to figures 4 and 5, for orientation I the solar radiation is taken to be incident along the X-axis of the satellite coordinate system. Thus the torque needs to be calculated only for the part of the orbit during which the satellite is in sunlight. The function  $f(\theta_n, \psi_m)$  appearing in equation (50) must be modified from the expression given in equation (43) by adding the photoelectric emission current, as used in equation (15)

$$j_p = 5 \times 10^{-5} \cos \psi \sin \theta \epsilon_p \quad (60)$$

where

$$\left. \begin{aligned} \epsilon_p &= 1 & (\cos \psi \geq 0) \\ \epsilon_p &= 0 & (\cos \psi < 0) \end{aligned} \right\} \quad (61)$$

The calculation of the current distribution and of the induction torque for the satellite with photoemission then proceeds the same as that for the uniformly conducting satellite without photoemission. The resulting torque for the uniformly conducting satellite with photoemission for orientation I is given in figure 17(a). Note that for one-half of the orbit the torque without photoemission is shown since during about one-half of the orbit the satellite is in the earth's shadow.

With reference to figures 4 and 5, the satellite orbit for orientation II is such that the solar radiation is incident along the Y-axis of the satellite coordinate system. The satellite will then remain in sunlight during the entire earth orbit. Now,  $f(\theta_n, \psi_m)$  must be modified from the expression given in equation (43) by adding

$$j_p = 5 \times 10^{-5} \sin \psi \sin \theta \epsilon'_p \quad (62)$$

where

$$\left. \begin{aligned} \epsilon'_p &= 1 & (\sin \psi \geq 0) \\ \epsilon'_p &= 0 & (\sin \psi < 0) \end{aligned} \right\} \quad (63)$$

The resulting torque for the uniformly conducting satellite with photoemission for orientation II is given in figure 17(b).

The torque for a spherical satellite made up of 106 gores is calculated next. It is assumed that the current flow is only along the gores. Also, the gores are connected near the poles so that the current can flow from one gore into another. For calculation of the torque the orientation of the satellite with respect to its spin axis is shown in figure 18.

The current in each gore must be determined. The current flowing into an element of surface of the nth gore is given by (see eqs. (5) and (10))

$$\begin{aligned}
 dI_n(\beta, \theta) = n_a e \left[ V_s \left( \frac{r_{\text{eff}}}{r_s} \right)^2 (\cos \beta \sin \theta \cos \psi_n - \sin \beta \cos \theta) \epsilon_i \right. \\
 \left. - \sqrt{\frac{kT}{2\pi m_e}} |\sin \theta \cos \psi_n \sin \alpha \right. \\
 \left. + \cos \alpha \cos \theta \left| \exp\left(\frac{e\phi_s \epsilon_\phi}{kT}\right) \right| \right] \Delta\psi r_s^2 \sin \theta \, d\theta \quad (64)
 \end{aligned}$$

where

$$\psi_n = n \Delta\psi = n \left( \frac{2\pi}{106} \right) \quad (n=0,1,2,\dots,105) \quad (65)$$

and  $\alpha$ ,  $\epsilon_i$ ,  $\epsilon_\phi$ , and  $\phi_s$  are given by equations (3), (11), (7), and (6), respectively. The total current flowing in the nth gore (in the  $\theta$ -direction) at  $\theta$  is then

$$i_n(\beta, \theta) = I_n(\beta, \theta) + I_n(\beta) \quad (66)$$

where

$$I_n(\beta, \theta) = \int_{\epsilon}^{\theta} dI_n(\beta, \theta) \quad (67)$$

and

$$I_n(\beta) = \frac{1}{R} [D(\beta) - \phi_n(\beta)] \quad (68)$$

$$R = \int_{\epsilon}^{\pi-\epsilon} \frac{S}{\Delta\psi \sin \theta} \, d\theta \quad (69)$$

$$\phi_n(\beta) = \int_{\epsilon}^{\pi-\epsilon} I_n(\beta, \theta) \frac{S}{\Delta\psi \sin \theta} \, d\theta \quad (70)$$

$$D(\beta) = \frac{1}{106} \sum_{n=0}^{105} \phi_n(\beta) \quad (71)$$

The resistance  $R$  as given in equation (69) is the resistance of one gore between the two ends where it is electrically connected to the other gores and  $\epsilon$  is the angle from the polar axis to the connecting ring as shown in figure 10. An additional current  $I_n(\beta)$  must flow in the  $n$ th gores of such magnitude that the voltage difference across that gore is equal to the average of the voltage differences across all gores due to the currents  $i_n(\beta, \theta)$ .

The force on an element of a gore  $d\vec{l}$  (fig. 18) is then given by

$$d\vec{F}_n = i_n(\beta, \theta) d\vec{l} \times \vec{B} \quad (72)$$

The corresponding torque is

$$d\vec{T}_n = \vec{r} \times d\vec{F}_n \quad (73)$$

The resulting torque on one of the gores is

$$\begin{aligned} \vec{T}_n(\beta) = r_s^2 B_a (1 + 3 \cos^2 \beta)^{1/2} & \left\{ \hat{i} \left[ \int_{\epsilon}^{\pi-\epsilon} \cos \theta \cos \psi_n (\sin \theta \cos \psi_n \sin \alpha \right. \right. \\ & + \cos \theta \cos \alpha) i_n(\theta, \beta) d\theta \left. \right] + \hat{j} \left[ \int_{\epsilon}^{\pi-\epsilon} \cos \theta \sin \psi_n (\sin \theta \cos \psi_n \sin \alpha \right. \\ & + \cos \alpha \cos \theta) i_n(\beta, \theta) d\theta \left. \right] - \hat{k} \left[ \int_{\epsilon}^{\pi-\epsilon} \sin \theta (\sin \theta \cos \psi_n \sin \alpha \right. \\ & \left. \left. + \cos \theta \cos \alpha) i_n(\beta, \theta) d\theta \right] \right\} \quad (74) \end{aligned}$$

By summing over all gores, the total torque becomes

$$T(\beta) = \sum_{n=0}^{105} T_n(\beta) \quad (75)$$

Equation (75) has been numerically integrated. The resulting torque as a function of  $\beta$  for Echo II without photoemission is shown in figure 19.

As was done for the uniformly conducting satellite, photoemission is next included and the induction torque is calculated for two orientations of the satellite orbit with respect to the earth-sun line. Again, for orientation I, the solar radiation is taken to be incident along the X-axis of the satellite coordinate system. Equation (64) must then be modified to

$$\begin{aligned}
 dI_n(\beta, \theta) = & \left[ n_a e V_s \left( \frac{r_{\text{eff}}}{r_s} \right)^2 (\cos \beta \sin \theta \cos \psi_n - \sin \beta \cos \theta) \epsilon_i \right. \\
 & - n_a e \sqrt{\frac{kT}{2\pi m_e}} |\sin \theta \cos \psi_n \sin \alpha + \cos \alpha \cos \theta| \exp\left(\frac{e\phi_s}{kT} \epsilon_\phi\right) \\
 & \left. + 5 \times 10^{-5} \sin \theta \cos \psi_n \epsilon_p \right] \Delta \psi r_s^2 \sin \theta d\theta \quad (76)
 \end{aligned}$$

With expression (76) being used for  $dI_n(\beta, \theta)$ , the method of calculating the induction torque for Echo II with photoemission is exactly the same as that for Echo II without photoemission. The resulting torque for Echo II with photoemission for orientation I is shown in figure 20(a).

For orientation II the solar radiation is incident along the Y-axis of the satellite coordinate system. Therefore, equation (64) must be modified to read

$$\begin{aligned}
 dI_n(\beta, \theta) = & \left[ n_a e V_s \left( \frac{r_{\text{eff}}}{r_s} \right)^2 (\cos \beta \sin \theta \cos \psi_n - \sin \beta \cos \theta) \epsilon_i \right. \\
 & - n_a e \sqrt{\frac{kT}{2\pi m_e}} |\sin \theta \cos \psi_n \sin \alpha + \cos \alpha \cos \theta| \exp\left(\frac{e\phi_s}{kT} \epsilon_\phi\right) \\
 & \left. + 5 \times 10^{-5} \sin \theta \sin \psi_n \epsilon_p \right] \Delta \psi r_s^2 \sin \theta d\theta \quad (77)
 \end{aligned}$$

The induction torque for Echo II with photoemission for orientation II is given in figure 20(b).

The induction torque for Echo II for the orientation shown in figure 12 should be calculated next. This induction-torque calculation is a much more arduous task than the calculation for the orientation shown in figure 11 inasmuch as the torques must be averaged at each satellite location over one complete revolution of the satellite about its spin axis. Because of the more difficult calculation and, also, because approximate calculations made by the author have shown that there is no appreciable difference in the induction torque for the two orientations, the induction torque is not calculated for the orientation shown in figure 12.

## OTHER POSSIBLE SOURCES OF TORQUE

Several phenomena other than the aforementioned ones may produce torques on the satellite. Torques may result from the density gradient in the atmosphere or from the radiation pressure. The resulting torques, however, are believed to be small compared with the eddy-current and the induction torques. The aerodynamic torque resulting from the spin should be calculated. Under the assumption that all neutral particles striking the satellite are diffusely reflected, the aerodynamic torque can be approximated by an expression given in reference 26 as (refer to figs. 4 and 5)

$$T_z \approx \frac{1}{2} \pi \rho v V_s r_s^4 |\cos \beta| \quad (78)$$

For values of  $\beta$  near  $\pi/2$ , equation (78) is no longer valid and the torque is given by (ref. 26)

$$T_z \approx \frac{2}{5} \pi \rho r_s^5 \omega^2 \quad (79)$$

The result for these approximations of the aerodynamic torque as applied to Echo II is shown in figure 21. In equation (79) the thermal motion of the ions has been neglected. The free molecule drag torque due to the thermal motion is given by Harbour and Lord (ref. 27) as

$$T_z = \frac{4}{5} r_s^2 n v \sqrt{2\pi m k T} = 4 \times 10^{-8} \text{ newton-meter} \quad (80)$$

The aerodynamic torque is quite small compared with the induction and the eddy-current torques.

## ELECTRIC CURRENTS IN SATELLITE SURFACE

The currents flowing in the surface of Echo II are due primarily to eddy currents, photoemission, and accretion of electrons and ions. To compare the various currents, a colatitude  $\beta$  of 0.7 radian was chosen. The eddy current (case I) flowing along a gore is, by equation (30),

$$i_\theta = -\frac{\omega}{R} r r_s^2 B \sin \alpha \cos \psi_n$$

This current is constant along a circular ring made up of two gores. For  $\beta = 0.7$  radian the currents in various gores are

$i_{\theta} = -4.2$ milliamperes	for $\psi_n = 0$
$i_{\theta} = -2.4$ milliamperes	for $\psi_n = 1.00$ radian
$i_{\theta} = -1.0$ milliamperes	for $\psi_n = 1.14$ radians
$i_{\theta} = -2.7$ milliamperes	for $\psi_n = 2.43$ radians

The corresponding induction currents without photoemission as determined from equation (66) are shown in figure 22. The induction current is not constant along a gore since it is determined by the accretion of electrons and ions by the satellite. The variation of the induction current for several gores with photoemission for orientation I and for orientation II is shown in figure 23.

The induction current densities for the uniformly conducting satellite without photoemission for several values of  $\theta'$  are shown in figure 24. For the uniformly conducting satellite two components of the surface current density must be determined since the current is no longer restricted to flow along the gores. Also, the induction current densities shown in figures 24 to 26 are referred to the satellite coordinate system shown in figure 14.

The variation of induction current density for the uniformly conducting satellite with photoemission for orientation I and for orientation II is shown in figures 25 and 26, respectively.

#### COMPARISON OF TORQUES

When comparing the torques it should be noted that all the torques are referred to the satellite coordinate system in figure 5. The results of the calculations indicate that only the eddy-current and the induction torques need be considered in attempting to find a balance of the torques acting on a satellite. The induction torque does not depend on the value of the surface resistivity  $S$  used in the calculations. For the uniformly conducting satellite,  $S$  does not even appear in the equations. For Echo II,  $D(\beta)$  and  $\phi_n(\beta)$  are both proportional to  $S$  and their difference is then divided by  $R$ , which is also proportional to  $S$ . By contrast, the eddy-current torque does depend on surface resistivity. However, if some of the connections between the connecting ring and the gores represent open circuits, then the value of the induction torque will change.

The average eddy-current torque for the uniformly conducting satellite over one earth orbit at  $\omega = 0.063$  radian per second is given in figure 8 as  $\langle T_z \rangle = 1.4 \times 10^{-3}$  newton-meter. The average torque for arbitrary  $\omega$  is therefore  $\langle T_z \rangle = -2.2 \times 10^{-2} \omega$  newton-meter. During at least one-half of the orbit the satellite will be exposed to sunlight. The value of the induction torque will thus be an average of the torques given in figures 17(a) and 17(b) - that

is,  $\langle T_z \rangle = -2.2 \times 10^{-5}$  newton-meter. The induction torque will balance the eddy-current torque for  $\omega = 10^{-3}$  radian per second or for a period of about 6280 seconds. Thus, for a uniformly conducting satellite of the same size and with the same orbit as Echo II, the equilibrium spin rate should be much less than that for Echo II. If the satellite is initially not spinning, then its rate of spin as determined by the eddy-current and induction torques will be given by

$$\omega = -10^{-3} \left[ 1 - \exp(-2.8 \times 10^{-7} t) \right] \quad (81)$$

The time constant involved in equation (81) is about 2 months.

The average eddy-current torque for Echo II over one earth orbit for the orientation shown in figure 10 is found from figure 11 to be  $8.6 \times 10^{-5}$  newton-meter. For the orientation shown in figure 12 the average eddy-current torque from figure 13 is  $4.3 \times 10^{-5}$  newton-meter. The actual eddy-current torque for Echo II should be bounded by these two values. For the induction torque the average of the values given in figures 20(a) and 20(b) - that is  $-3.7 \times 10^{-5}$  newton-meter - should be used. It will be noted that the eddy-current torque and the induction torque are of the same order of magnitude. Thus, considering the uncertainties in the electrical properties of Echo II, the agreement between the accelerating and retarding torques is good.

The exact value of the induction torque will depend on which gores are electrically connected to the connection ring and which are not. For example, if every other gore is not connected to the top connecting ring (see fig. 9), then for a value of  $\beta = 5.97$  radians the induction torques are

Without photoemission:

$$T_z = -5.8 \times 10^{-5} \text{ newton-meter}$$

With photoemission, orientation II:

$$T_z = -1.5 \times 10^{-4} \text{ newton-meter}$$

For the results presented in figures 19 and 20, the corresponding torques under conditions where all gores are electrically connected to the connecting ring are

Without photoemission:

$$T_z = -1.3 \times 10^{-5} \text{ newton-meter}$$

With photoemission, orientation II:

$$T_z = -1.1 \times 10^{-4} \text{ newton-meter}$$

However, when the average torque over one earth orbit is computed for the satellite with open circuits as previously defined, only a slight increase in the induction torque is obtained. It is the author's opinion that any other arrangement of open circuits will not appreciably increase the average induction torque. Therefore, when electrical continuity is considered, the eddy-current torque and the induction torque are found to be nearly equal in magnitude. An interesting factor in the spin history of Echo II is that the spin rate increases slightly during the periods when the satellite orbit is 100 percent in sunlight. These observations are in agreement with the results presented in figures 19 and 20 where the induction torque is much larger in the presence of photoemission.

It is of interest to find the time in which Echo II would achieve a steady spin rate if  $\omega$  were zero initially. Note that since the induction torque is negative for Echo II, the final  $\omega$  also will be negative. For the results given in figure 11 (case I), the eddy-current torque for arbitrary  $\omega$  is  $1.4 \times 10^{-3}\omega$  newton-meter. Therefore, the spin rate of Echo II as determined by the eddy-current and induction torques is given by

$$\omega = -2.7 \times 10^{-2} \left[ 1 - \exp(-1.75 \times 10^{-8}t) \right] \quad (82)$$

The time constant involved in equation (82) is about 22 months.

If the eddy-current torque for the orientation shown in figure 12 (case II) is used and if the average induction torque is assumed to remain unchanged from the previous orientation, then equation (82) becomes

$$\omega = -5.3 \times 10^{-2} \left[ 1 - \exp(-8.8 \times 10^{-9}t) \right] \quad (83)$$

The time constant involved in equation (83) is about 44 months.

Table II summarizes the different torques for Echo II and for the uniformly conducting satellite at the rate of spin indicated.

#### CONCLUDING REMARKS

It was found that only the eddy-current torque and the induction torque had to be considered in obtaining a balance of the accelerating and the retarding torques. For Echo II (1964 4A) the calculated equilibrium rate of spin is between  $-2.7 \times 10^{-2}$  and  $-5.3 \times 10^{-2}$  radian per second which is close to the observed spin rate of  $-6.3 \times 10^{-2}$  radian per second. Therefore, the probable explanation of the constancy of the rate of spin of Echo II is that the eddy-current torque and the induction torque were in balance and that all other torques were negligible. Also, since the induction torque is negative, the spin axis should point in the negative z-direction.

It should be noted that Echo II was spinning at a rate of about 1 revolution per 100 seconds for 9 months after launching. It is also known that this spin rate was established during the first orbit. In the light of the present analysis, however, it is hard to escape the conclusion that the initial spin vector only by chance closely approximated the equilibrium spin vector.

The surface current was found to be of the order of several milliamperes per meter. Whether currents of this magnitude would interfere with experiments onboard a satellite will depend on the particular experiment to be performed.

Langley Research Center,  
National Aeronautics and Space Administration,  
Langley Station, Hampton, Va., November 1, 1965.

## APPENDIX

### COMPARISON OF EFFECTIVE SATELLITE RADII

By use of the method given by Hohl and Wood in reference 10 the potential distribution and the ion trajectories have been calculated for two values of  $\beta$  (without photoemission). The potential distribution is shown in figures 27(a) and 27(b) for  $\beta = 0.4$  and 1.39 radians, respectively. The corresponding ion trajectories in the plane defined by the satellite velocity vector and the Y-axis of the satellite coordinate system (fig. 5) are shown in figures 28(a) and 28(b).

Considering the trajectories given in figure 28(a) values obtained for  $\delta$  are 7 and 0 Debye lengths for  $\theta = 0$  and  $\theta = \pi$ , respectively. The corresponding values obtained by using the result of Jastrow and Pearse (eq. (9)) are 5.5 and 0 Debye lengths. For  $\beta = 1.39$ , values of  $\delta$  obtained from figure 28(b) are 12 and -1.1 Debye lengths, whereas the corresponding values obtained from equation (9) are 15 and -2 Debye lengths.

## REFERENCES

1. Warwick, J. W.: Decay of Spin in Sputnik I. *Planetary Space Sci.*, vol. 1, no. 1, Jan. 1959, pp. 43-49.
2. Hanson, W. B.: Upper-Atmosphere Helium Ions. *J. Geophys. Res.*, vol. 67, no. 1, Jan. 1962, pp. 183-188.
3. Hanson, W. B.: Structure of the Ionosphere. *Satellite Environment Handbook*, Second ed., Francis S. Johnson, ed., Stanford Univ. Press, 1965, pp. 21-49.
4. Johnson, Francis S.: Atmospheric Structure. *Astronautics*, vol. 7, no. 8, Aug. 1962, pp. 54-61.
5. Johnson, Francis S.: Structure of the Upper Atmosphere. *Satellite Environment Handbook*, Second ed., Francis S. Johnson, ed., Stanford Univ. Press, 1965, pp. 1-20.
6. Walker, James C. G.: The Upper Atmosphere. *Space/Aeron.*, vol. 42, no. 5, Oct. 1964, pp. 56-63.
7. Bourdeau, Robert E.: Research Within the Ionosphere. *Science*, vol. 148, no. 3670, Apr. 30, 1965, pp. 585-594.
8. Spitzer, Lyman, Jr.: *Physics of Fully Ionized Gases*. Second rev. ed., Interscience Publ., 1962.
9. Bourdeau, R. E.; Whipple, E. C., Jr.; Donley, J. L.; and Bauer, S. J.: Experimental Evidence for the Presence of Helium Ions Based on Explorer VIII Satellite Data. *J. Geophys. Res.*, vol. 67, no. 2, Feb. 1962, pp. 467-475.
10. Hohl, Frank; and Wood, George P.: The Electrostatic and Electromagnetic Drag Forces on a Spherical Satellite in a Rarefied Partially Ionized Atmosphere. *Rarefied Gas Dynamics*, Vol. II, J. A. Laurmann, ed., Academic Press, 1963, pp. 45-64.
11. Hagstrum, Homer D.: Auger Ejection of Electrons From Tungsten by Noble Gas Ions. *Phys. Rev.*, vol. 96, no. 2, Oct. 15, 1954, pp. 325-335.
12. Hagstrum, Homer D.: Theory of Auger Ejection of Electrons From Metals by Ions. *Phys. Rev.*, vol. 96, no. 2, Oct. 15, 1954, pp. 336-365.
13. Hagstrum, Homer D.: Auger Ejection of Electrons From Molybdenum by Noble Gas Ions. *Phys. Rev.*, vol. 104, no. 3, Nov. 1, 1956, pp. 672-683.
14. Dessler, A. J.: Geomagnetism. *Satellite Environment Handbook*, Second ed., Francis S. Johnson, ed., Stanford Univ. Press, 1965, pp. 151-182.

15. Wood, George P.; and Hohl, Frank: Electric Potentials, Forces and Torques on Bodies Moving Through Rarefied Plasmas. Paper No. 65-628, Am. Inst. Aeron. Astronaut., Aug. 1965.
16. Bourdeau, R. E.; Donley, J. L.; Serbu, G. P.; and Whipple, E. C., Jr.: Measurements of Sheath Currents and Equilibrium Potential on the Explorer VIII Satellite. J. Astronaut. Sci., vol. VIII, no. 3, Fall 1961, pp. 65-73.
17. Jastrow, R.; and Pearse, C. A.: Atmospheric Drag on the Satellite. J. Geophys. Res., vol. 62, no. 3, Sept. 1957, pp. 413-423.
18. Chang, H. H. C.; and Smith, M. C.: On the Drag of a Spherical Satellite Moving in a Partially Ionized Atmosphere. J. Brit. Interplanet. Soc., vol. 17, no. 7, Jan.-Feb. 1960, pp. 199-205.
19. Brundin, Clark L.: Effects of Charged Particles on the Motion of an Earth Satellite. AIAA J., vol. 1, no. 11, Nov. 1963, pp. 2529-2538.
20. Stratton, Julius Adams: Electromagnetic Theory. McGraw-Hill Book Co., Inc., 1941.
21. Smythe, William R.: Static and Dynamic Electricity. McGraw-Hill Book Co., Inc., 1950.
22. Vinti, John P.: Theory of the Spin of a Conducting Satellite in the Magnetic Field of the Earth. Rept. No. 1020, Ballistic Res. Labs., Aberdeen Proving Ground, July 1957.
23. Smith, G. Louis: A Theoretical Study of the Torques Induced by a Magnetic Field on Rotating Cylinders and Spinning Thin-Wall Cones, Cone Frustums, and General Body of Revolution. NASA TR R-129, 1962.
24. Zonov, Yu. V.: On the Problem of the Interaction Between a Satellite and the Earth's Magnetic Field. NASA TT F-37, 1960.
25. Halverson, R. P.; and Cohen, H.: Torque on a Spinning Hollow Sphere in a Uniform Magnetic Field. IEEE, Trans. Aerospace Navigational Electron., vol. ANE-11, June 1964, pp. 118-127.
26. Davis, R. J.; Whipple, F. L.; and Zirker, J. B.: The Orbit of a Small Earth Satellite. Scientific Uses of Earth Satellites, James A. Van Allen, ed., Univ. of Michigan Press, c.1956, pp. 1-22.
27. Harbour, P. J.; and Lord, R. G.: A Rotating Sphere, Absolute Vacuum Gauge. J. Sci. Instr., vol. 42, no. 2, Feb. 1965, pp. 105-108.

TABLE I.- ATMOSPHERE AND SATELLITE PARAMETERS

AT 1200-KILOMETER ALTITUDE

Atmosphere:

Total mass density, $\text{kg/m}^3$ . . . . .	$10^{-15}$
Ion mass density, $\text{kg/m}^3$ . . . . .	$10^{-16}$
Ion or electron number density, $\text{m}^{-3}$ . . . . .	$10^{10}$
Ion temperature, $^{\circ}\text{K}$ . . . . .	$10^3$
Electron temperature, $^{\circ}\text{K}$ . . . . .	$1.6 \times 10^3$
Debye length, m . . . . .	$2.7 \times 10^{-2}$
Ion ( $\text{He}^+$ ) thermal velocity, m/sec . . . . .	$2.5 \times 10^3$
Electron thermal velocity, m/sec . . . . .	$2.7 \times 10^5$
Ion mean free path, m . . . . .	$2.6 \times 10^4$
Electron mean free path, m . . . . .	$3.2 \times 10^4$
Ion radius of gyration, m . . . . .	3.6
Electron radius of gyration, m . . . . .	$5.1 \times 10^{-2}$
Revolutions per collision for ions . . . . .	$1.1 \times 10^3$
Revolutions per collision for electrons . . . . .	$10^5$
Magnetic field (over magnetic pole), $\text{Wb/m}^2$ . . . . .	$3.8 \times 10^{-5}$

Echo II:

Velocity, m/sec . . . . .	$7.3 \times 10^3$
Radius, m . . . . .	20.5
Spin rate, rad/sec . . . . .	$6.3 \times 10^{-2}$
Moment of inertia, $\text{kg-m}^2$ . . . . .	$7.96 \times 10^4$
Surface resistivity, $\Omega$ . . . . .	$6.7 \times 10^{-3}$
Mass, kg . . . . .	252.9
Temperature, $^{\circ}\text{K}$ . . . . .	313

TABLE II.- AVERAGE OF TORQUES OVER ONE EARTH ORBIT  $\langle T_z \rangle$

Torque	Echo II ( $\omega = -6.3 \times 10^{-2}$ rad/sec)	Uniformly conducting satellite ( $\omega = -10^{-3}$ rad/sec)
Eddy-current torque, N-m . . .	$4.3 \times 10^{-5}$ to $8.6 \times 10^{-5}$	$2.2 \times 10^{-5}$
Surface charge torque, N-m . .	$3.8 \times 10^{-8}$	$6 \times 10^{-23}$
Aerodynamic torque, N-m . . .	$8.2 \times 10^{-8}$	$1.3 \times 10^{-9}$
Induction torque, N-m . . . .	$-3.7 \times 10^{-5}$	$-2.2 \times 10^{-5}$
Coulomb torque, N-m . . . . .	$-7 \times 10^{-7}$	$-7 \times 10^{-7}$

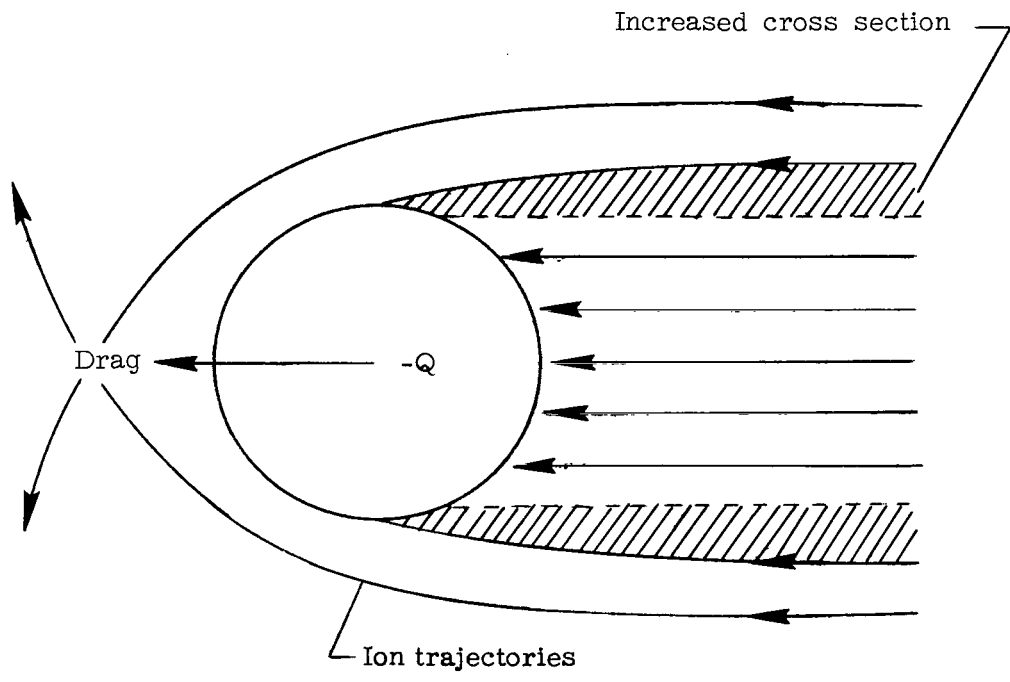


Figure 1.- Coulomb drag only, no torque.

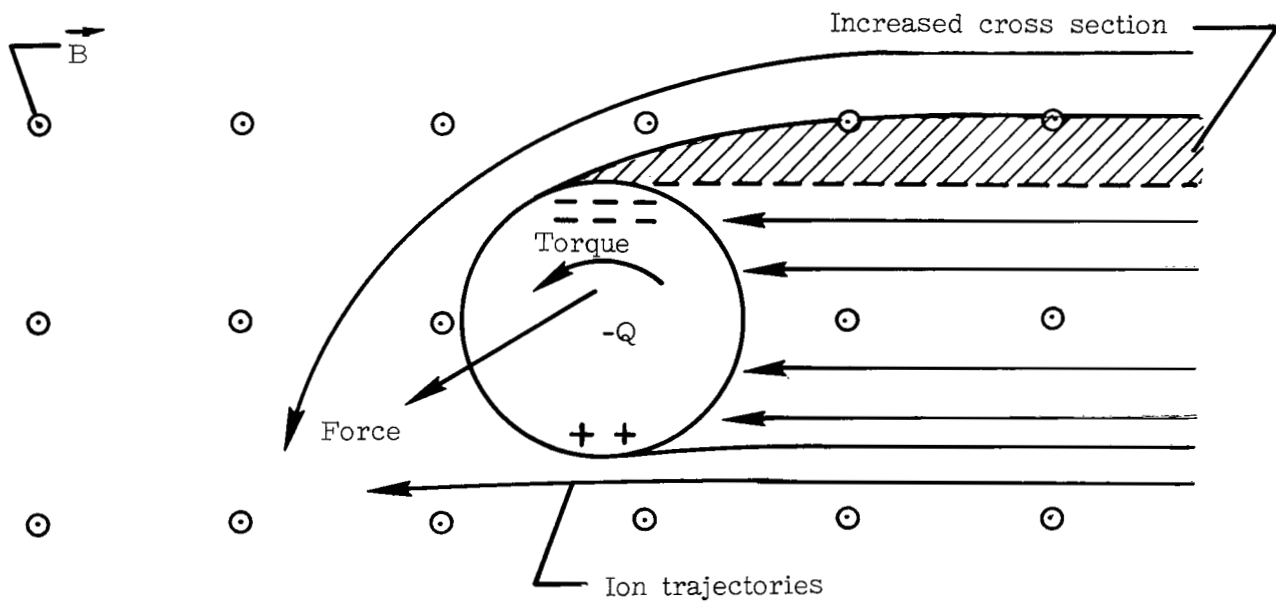


Figure 2.- Coulomb force and Coulomb torque.

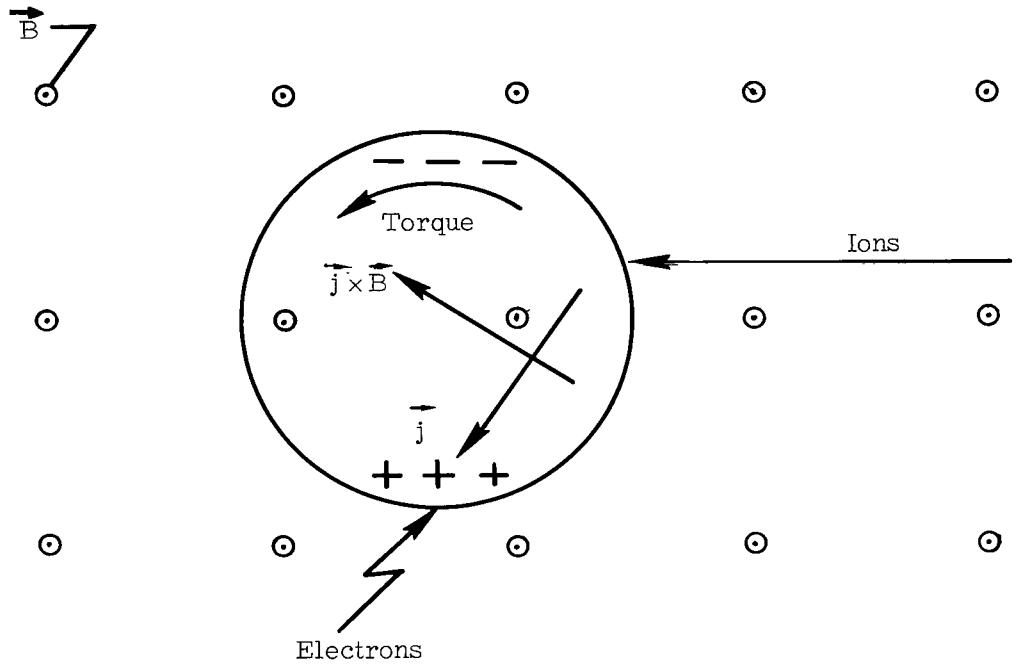


Figure 3.- Induction torque.

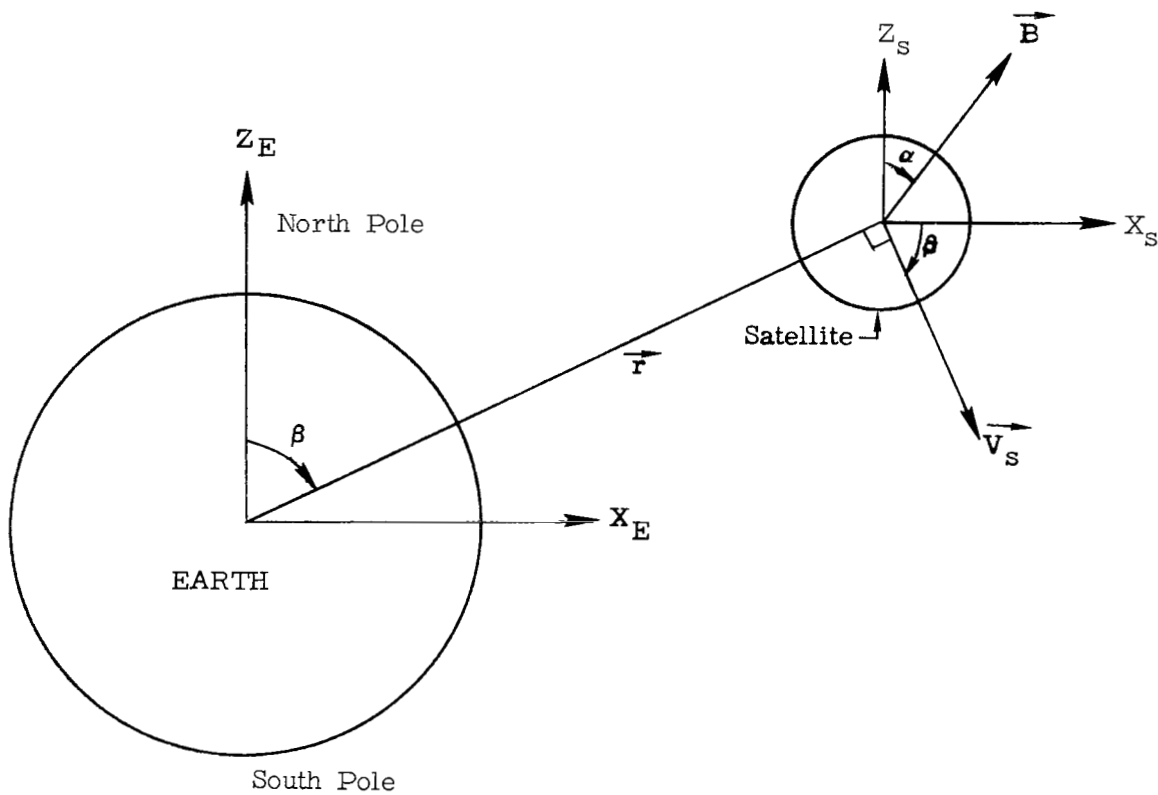


Figure 4.- Satellite orientation with respect to the earth.

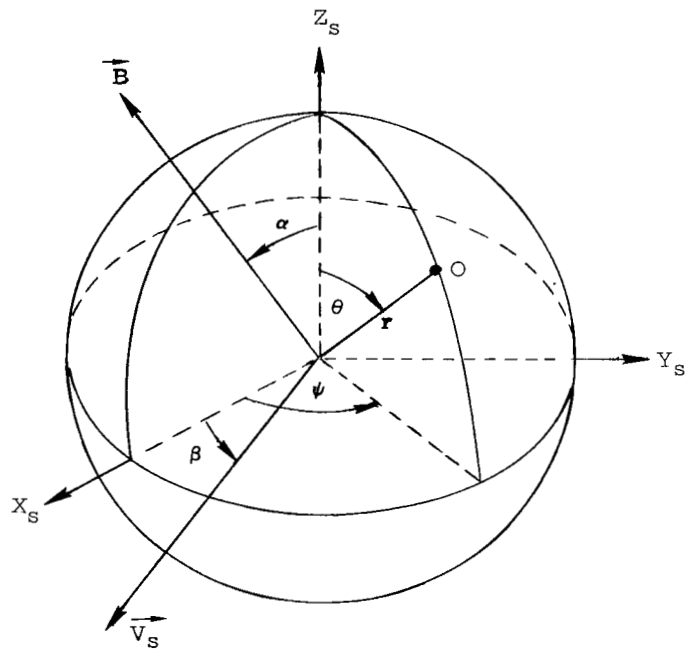


Figure 5.- Spherical and Cartesian coordinate systems used for finding  $\phi_{eq}$ .

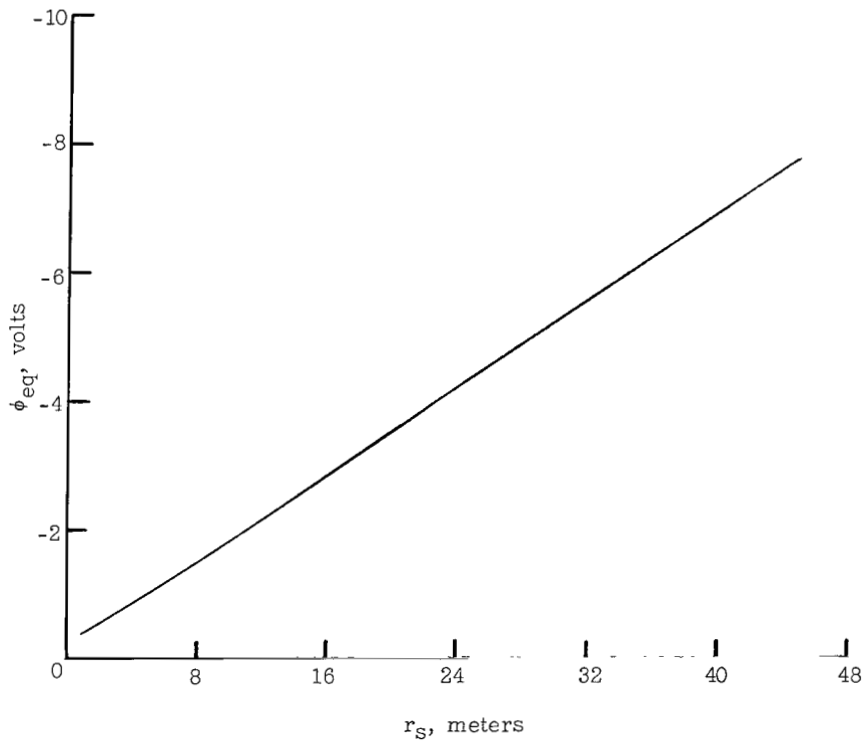
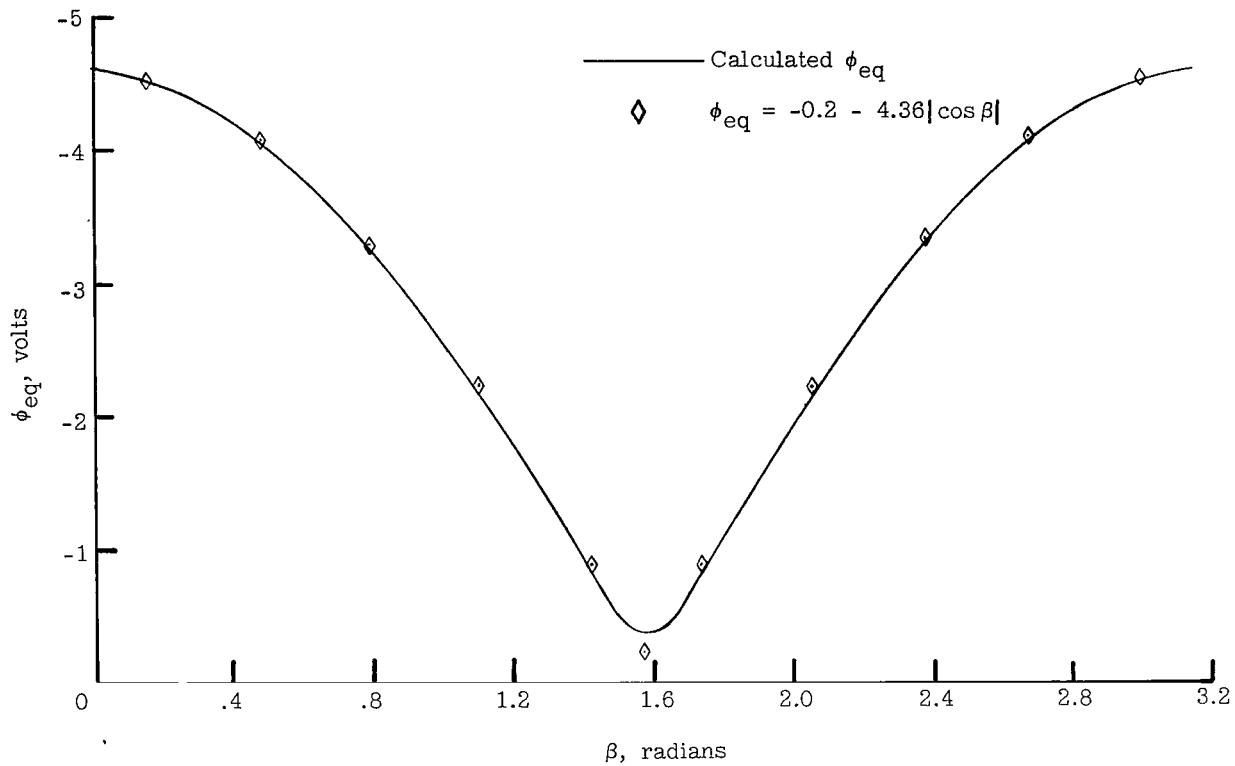
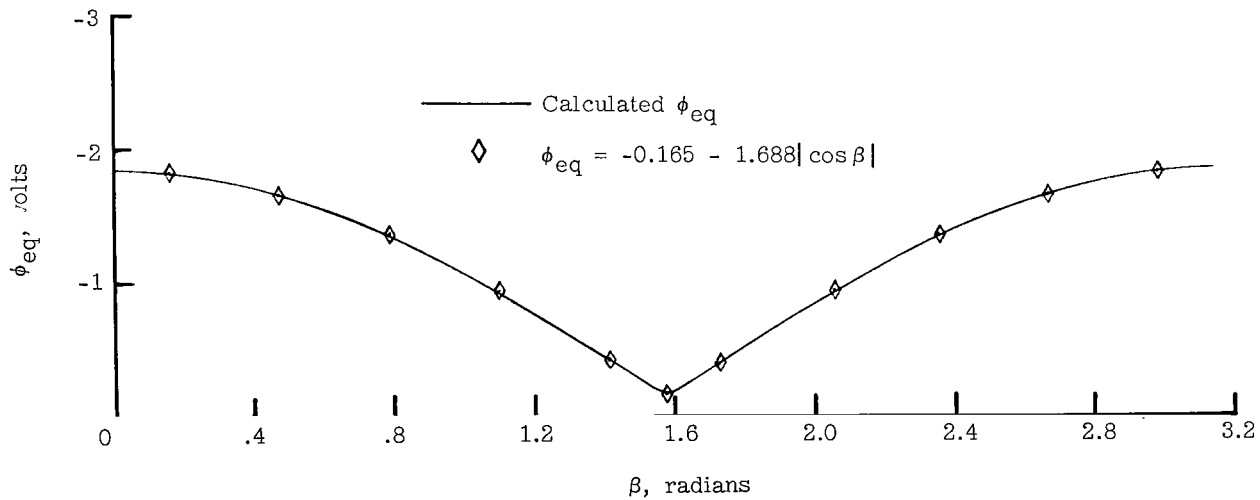


Figure 6.- Equilibrium potential  $\vec{\phi}_{eq}$  without photoemission as a function of satellite radius.  
 $\vec{V}_S \times \vec{B} = 0.22$  volt/meter.



(a) Without photoemission.



(b) With photoemission.

Figure 7.- Equilibrium potential as a function of colatitude for Echo II.

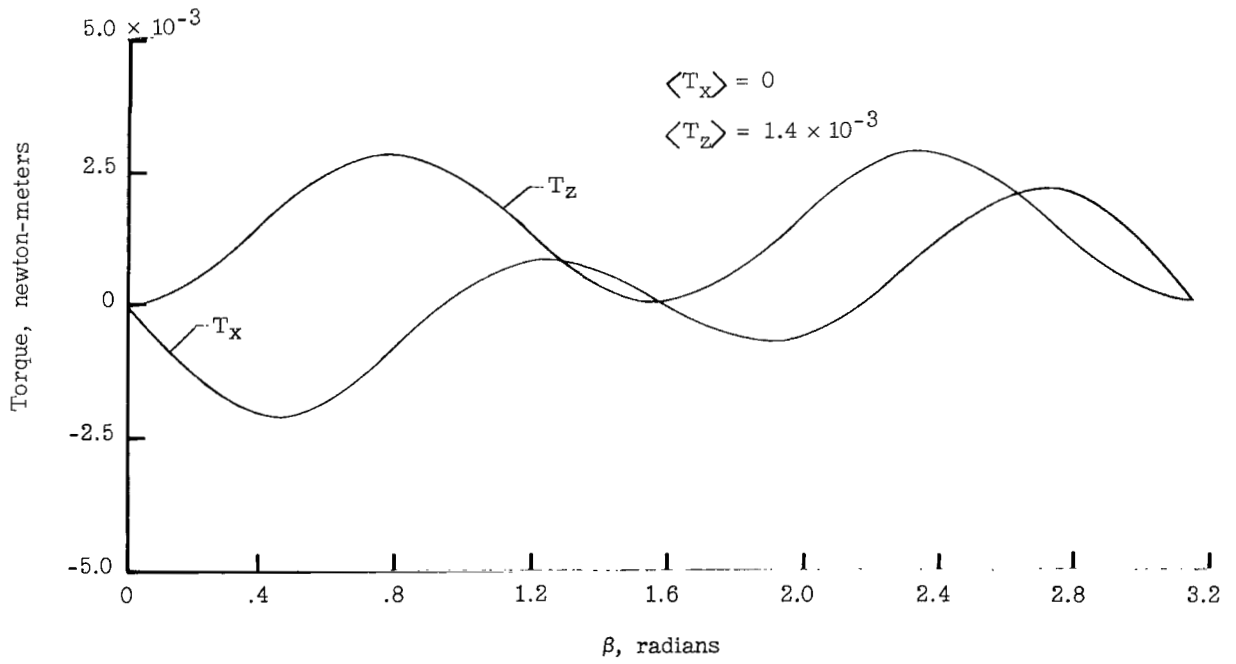
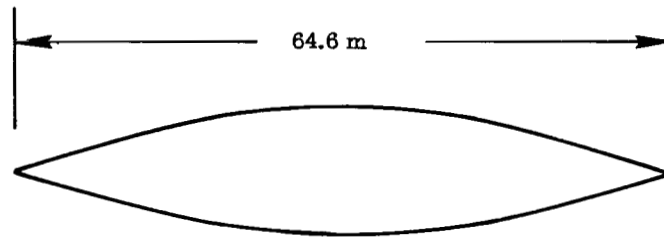
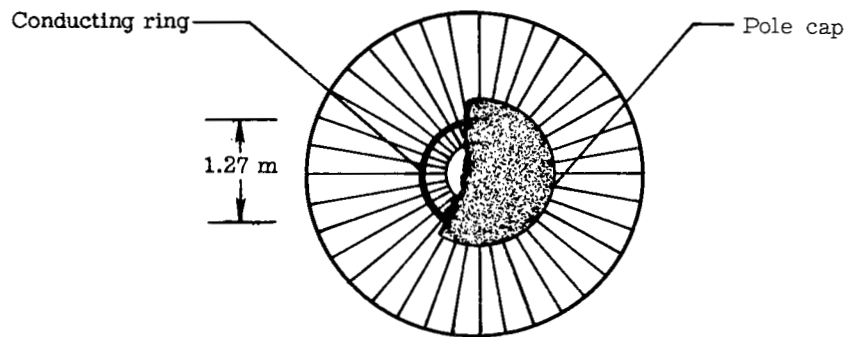


Figure 8.- Eddy-current torque for uniformly conducting spherical shell.



(a) Gore.



(b) Polar end construction.

Figure 9.- Construction of Echo II satellite.

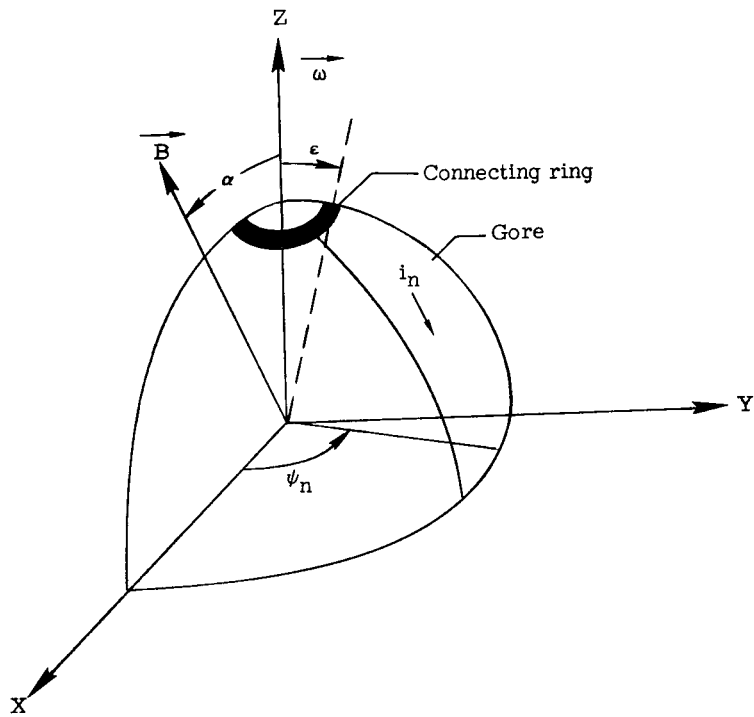


Figure 10.- Satellite orientation for calculation of eddy-current torque. Case I.

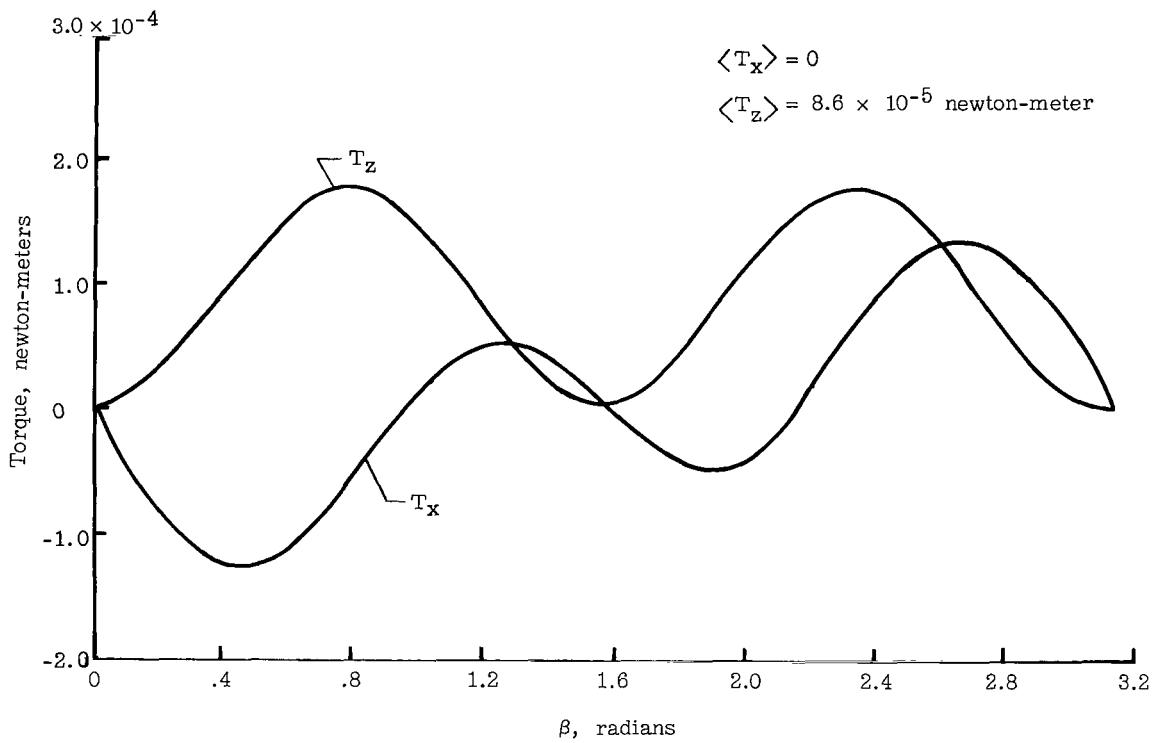


Figure 11.- Eddy-current torque for Echo II. Case I.

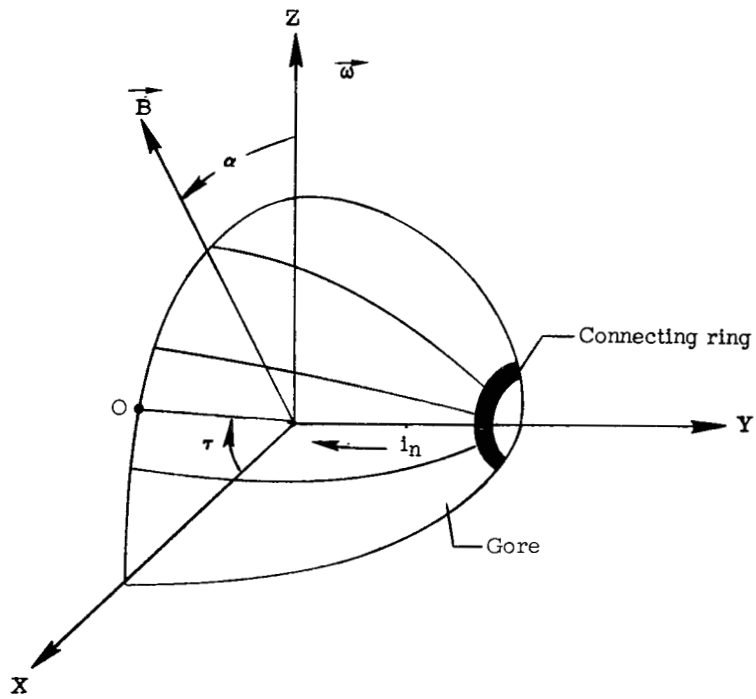


Figure 12.- Satellite orientation for calculation of eddy-current torque. Case II.

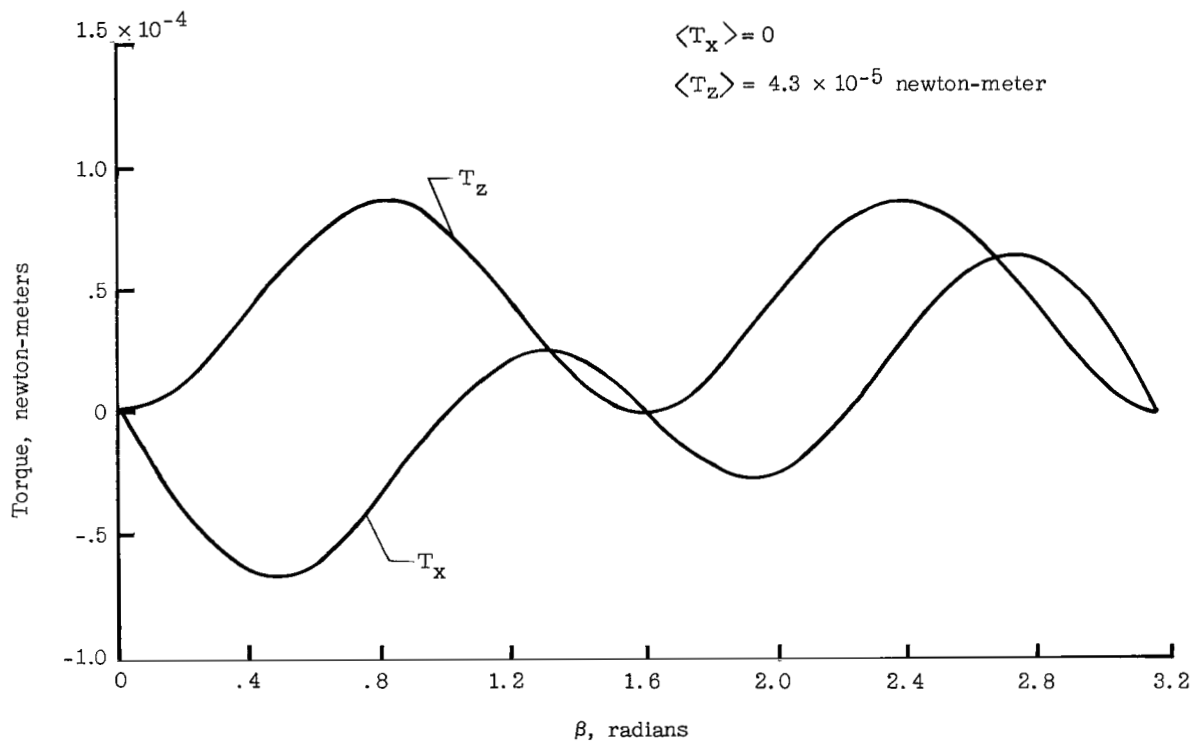


Figure 13.- Eddy-current torque for Echo II. Case II.

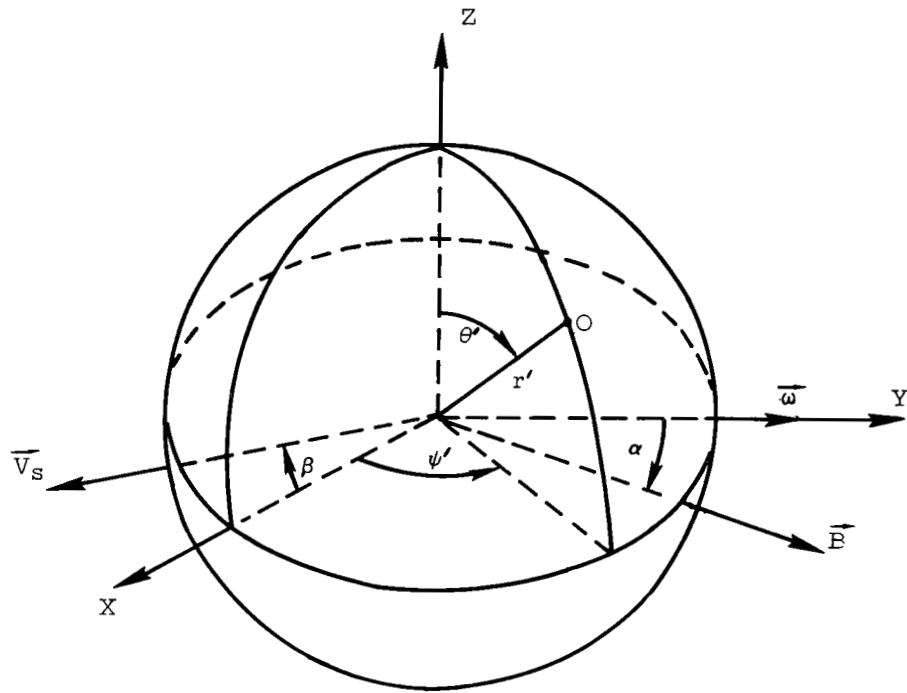


Figure 14.- Coordinate system used for calculating Coulomb torque.

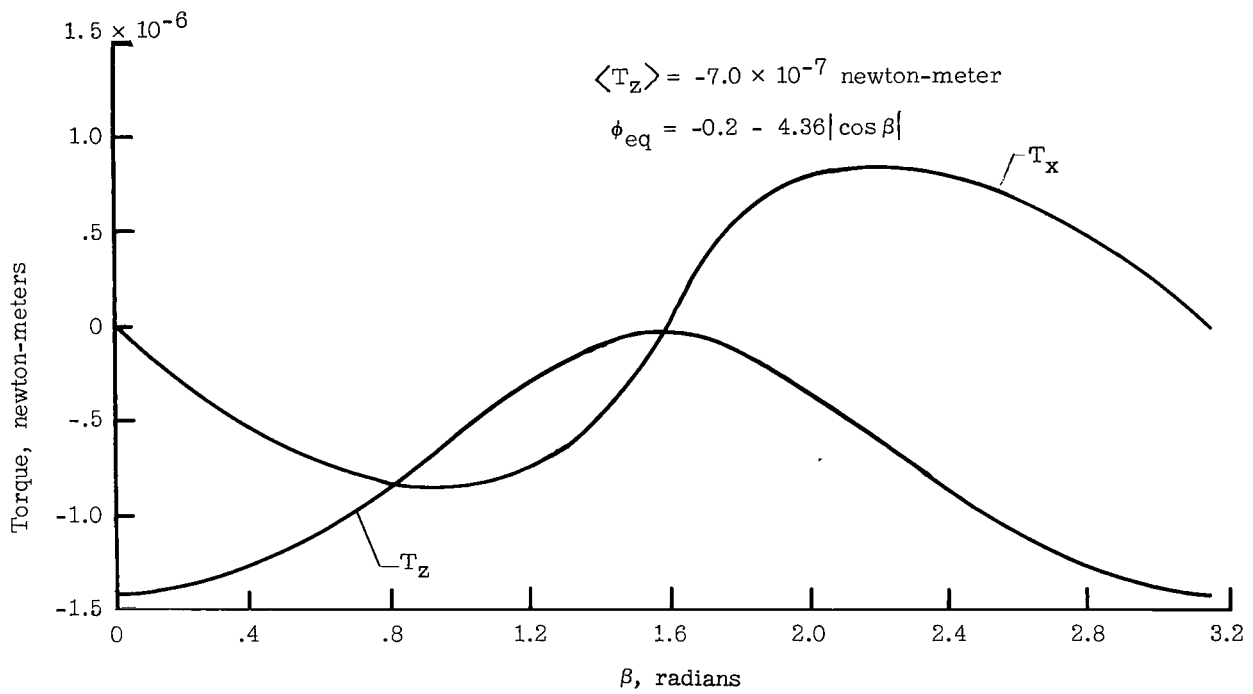


Figure 15.- Coulomb torque for Echo II.

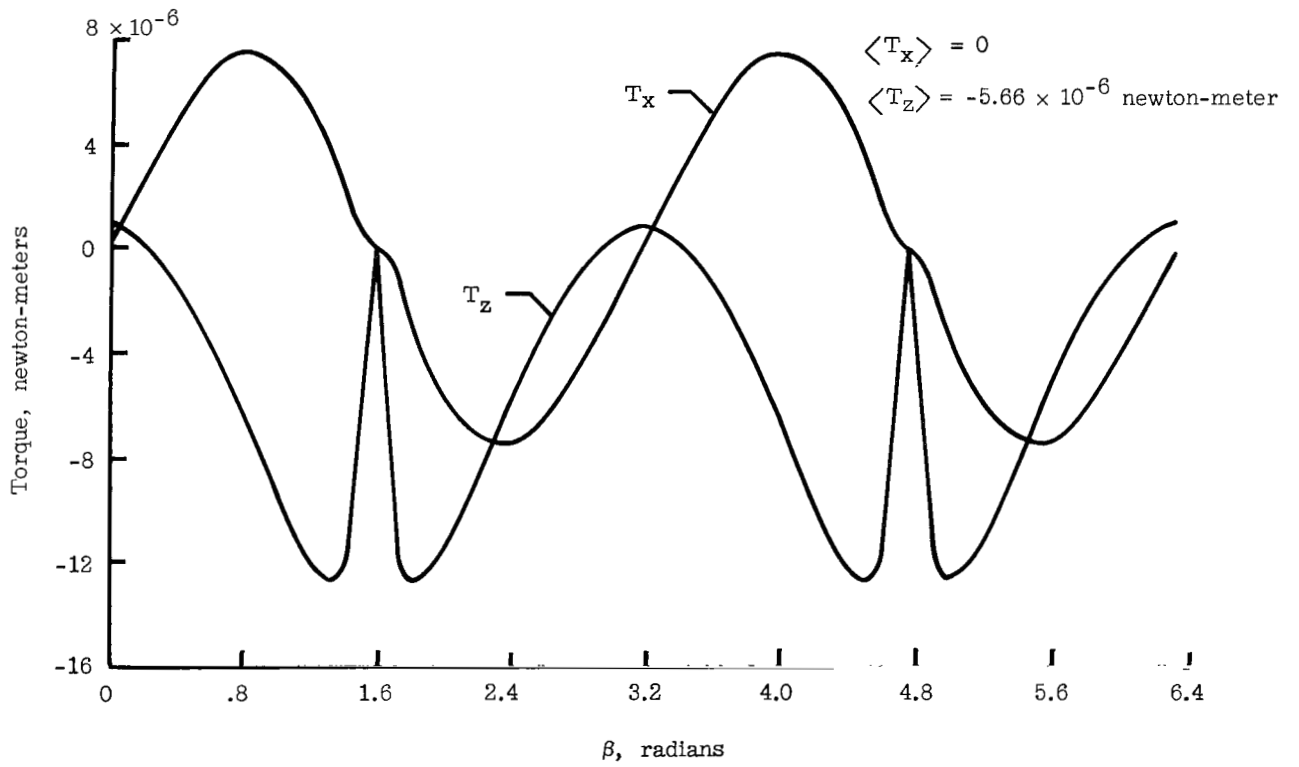
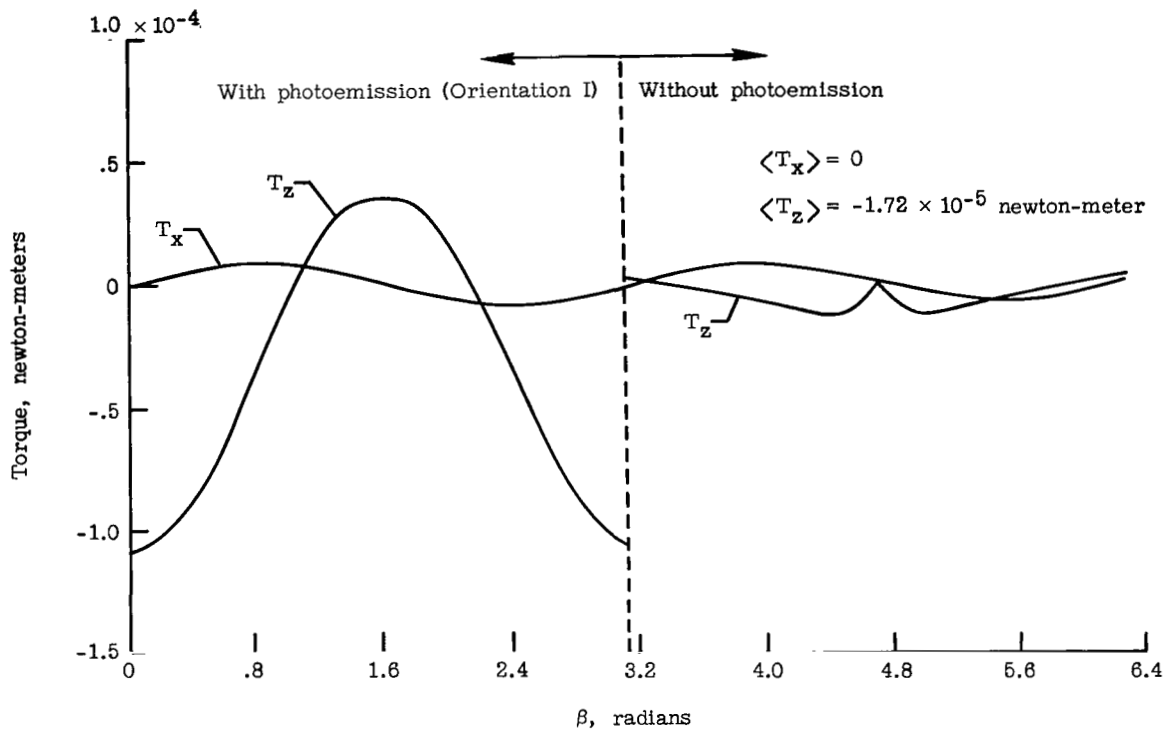
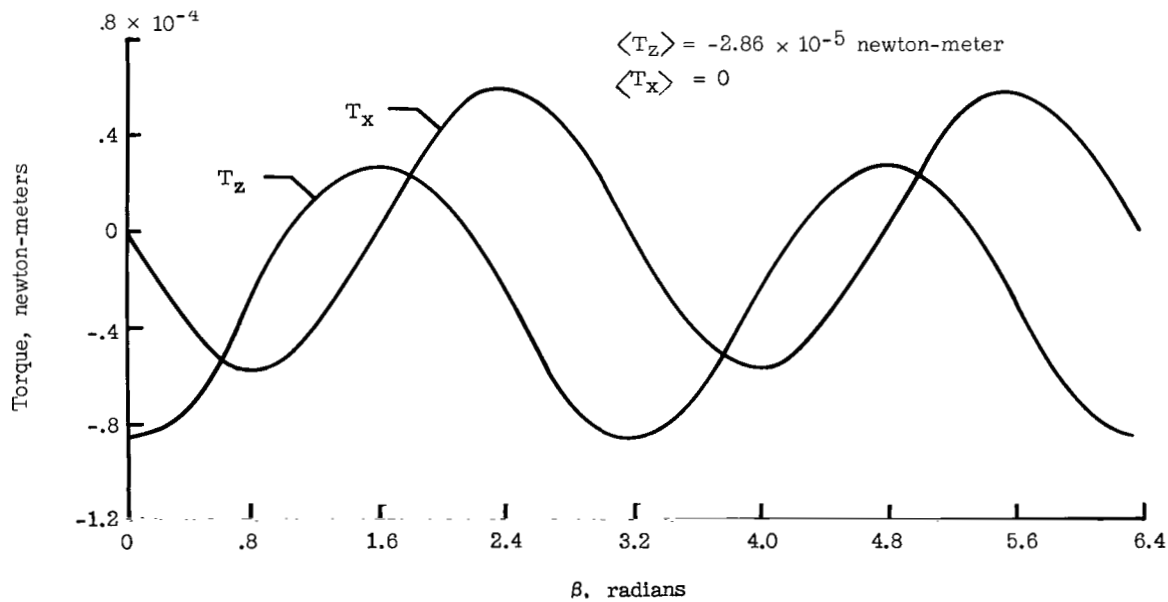


Figure 16.- Induction torque for uniformly conducting satellite without photoemission.



(a) Orientation I.



(b) Orientation II.

Figure 17.- Induction torque for uniformly conducting satellite with photoemission.

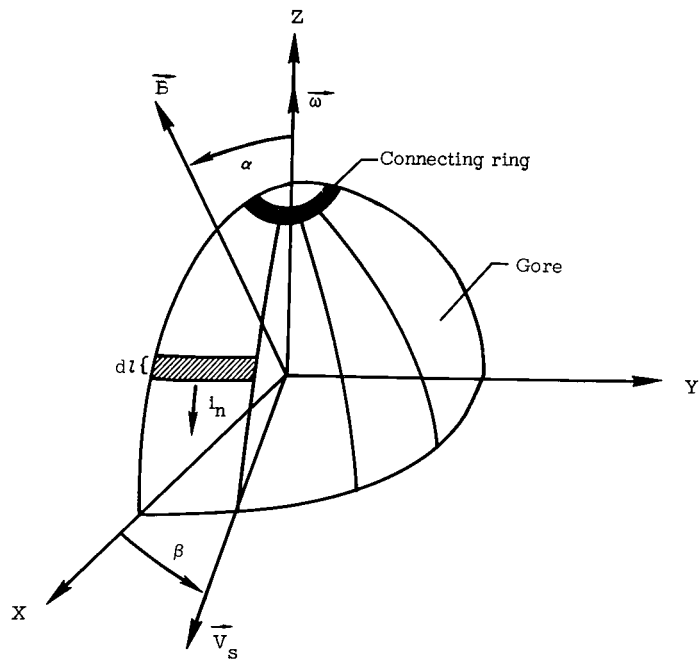


Figure 18.- Orientation of gores for calculating induction torque.

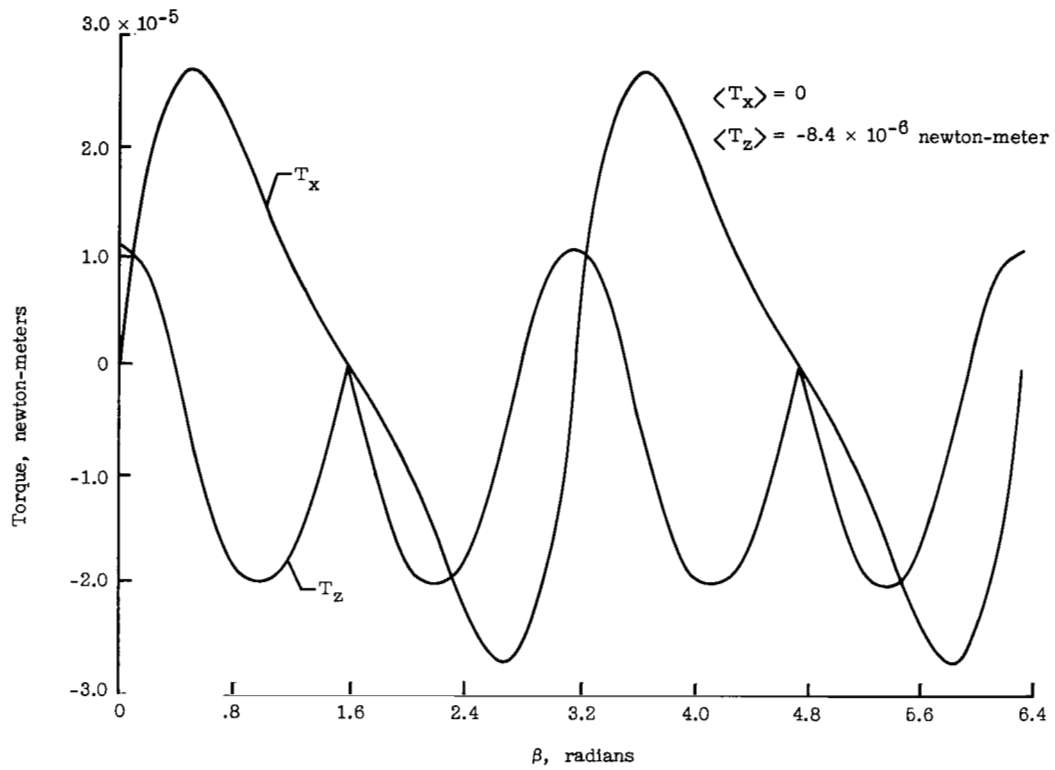
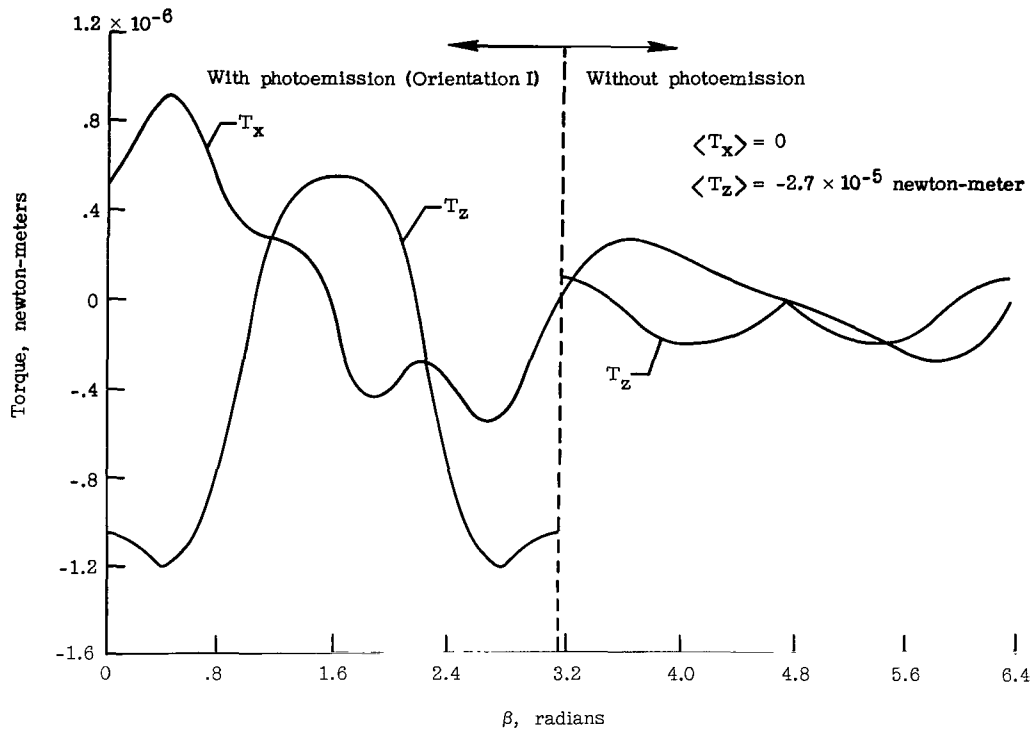
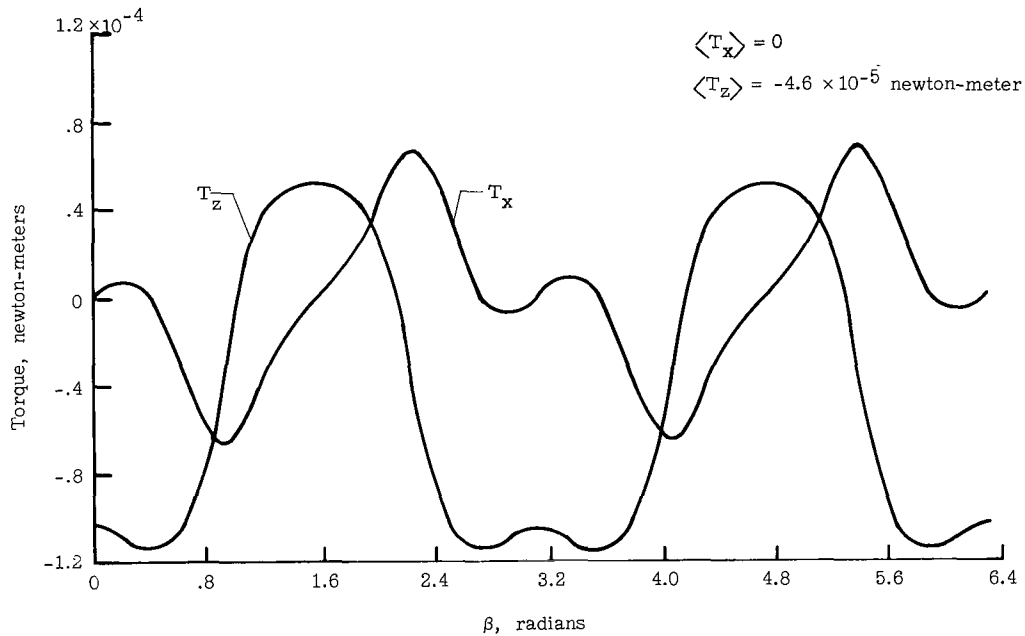


Figure 19.- Induction torque for Echo II without photoemission.



(a) Orientation I.



(b) Orientation II.

Figure 20.- Induction torque for Echo II with photoemission.

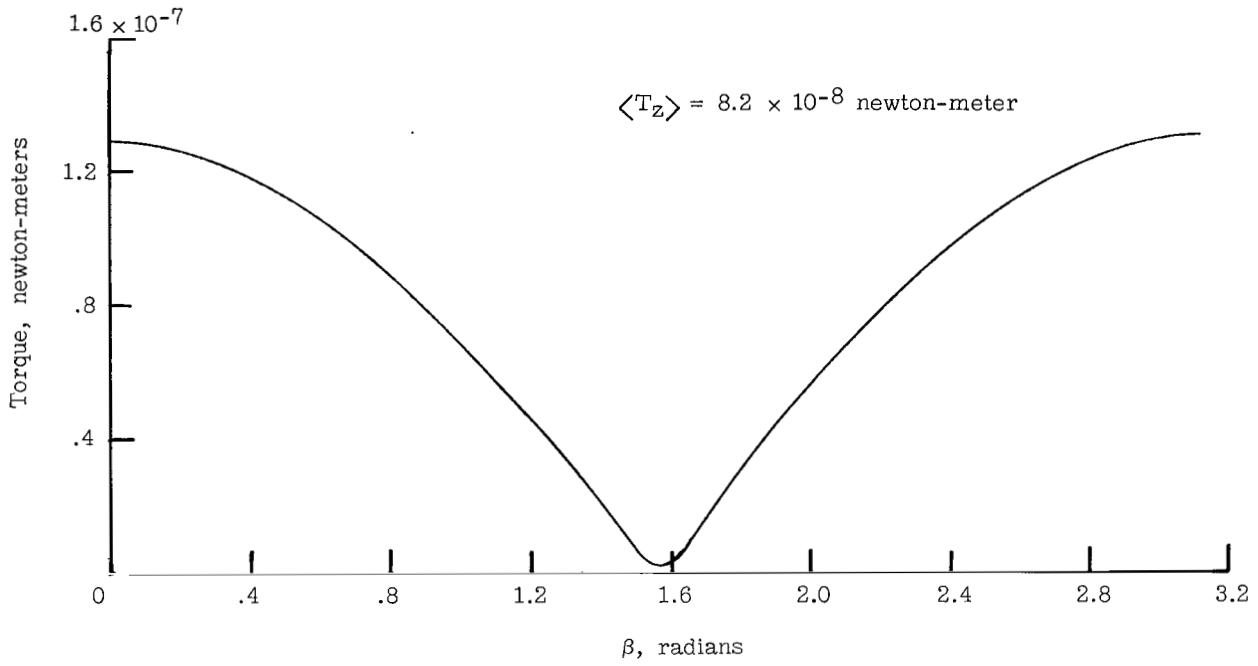


Figure 21.- Aerodynamic torque of Echo II.

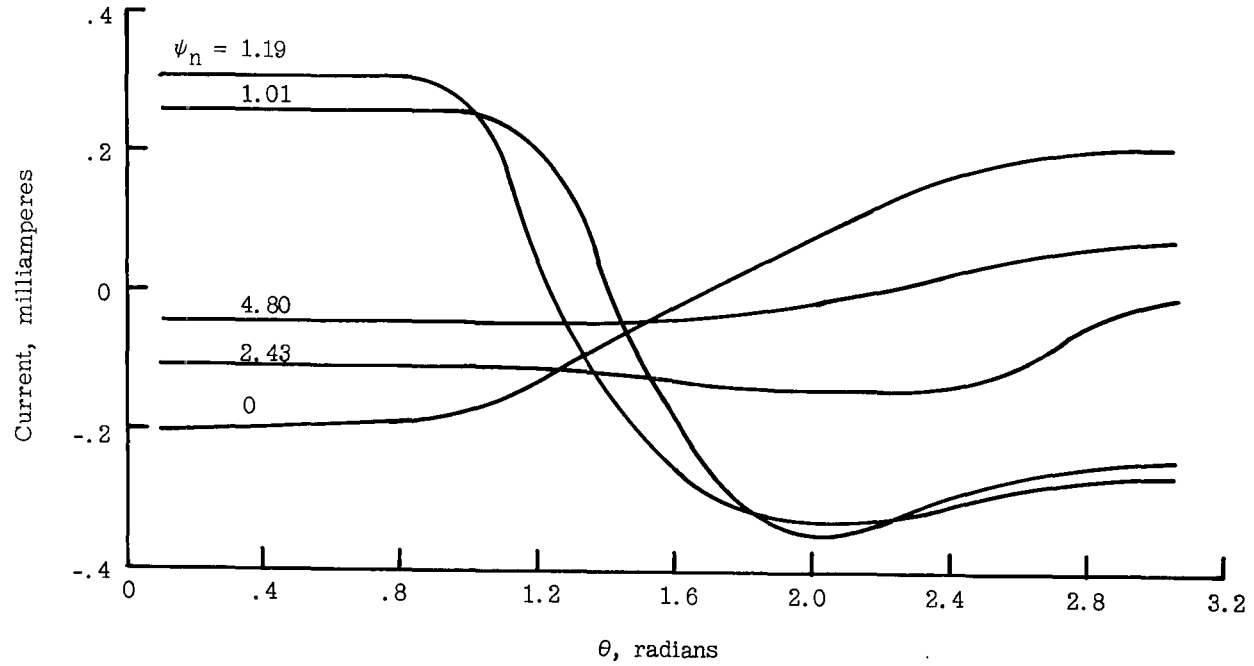
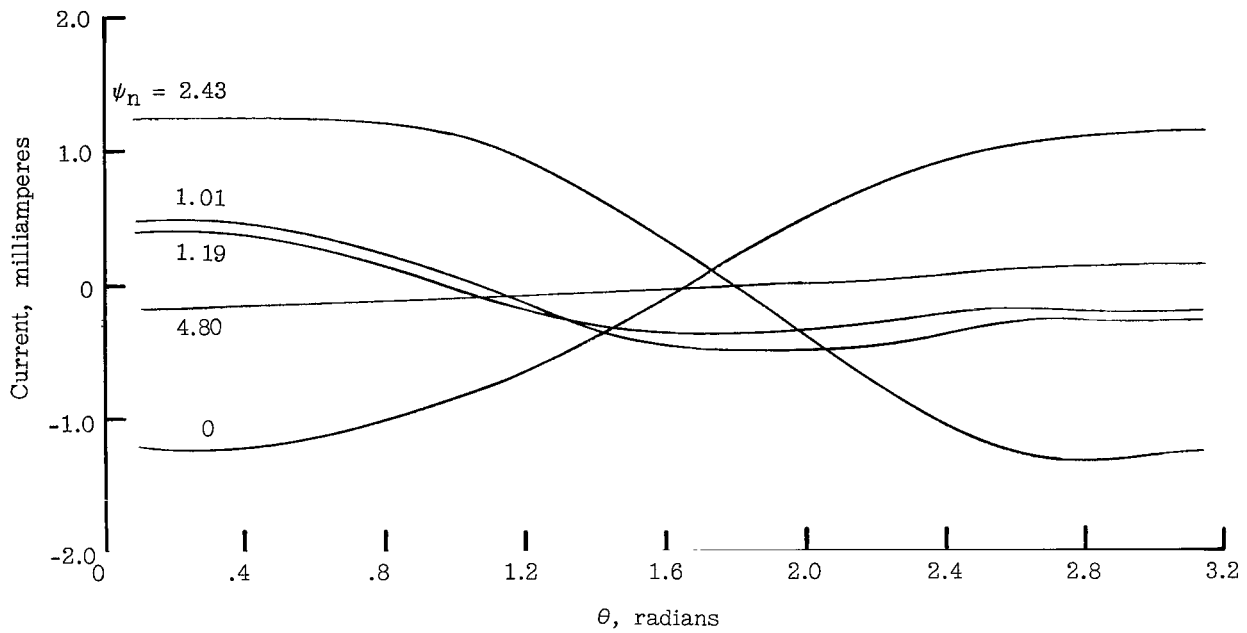
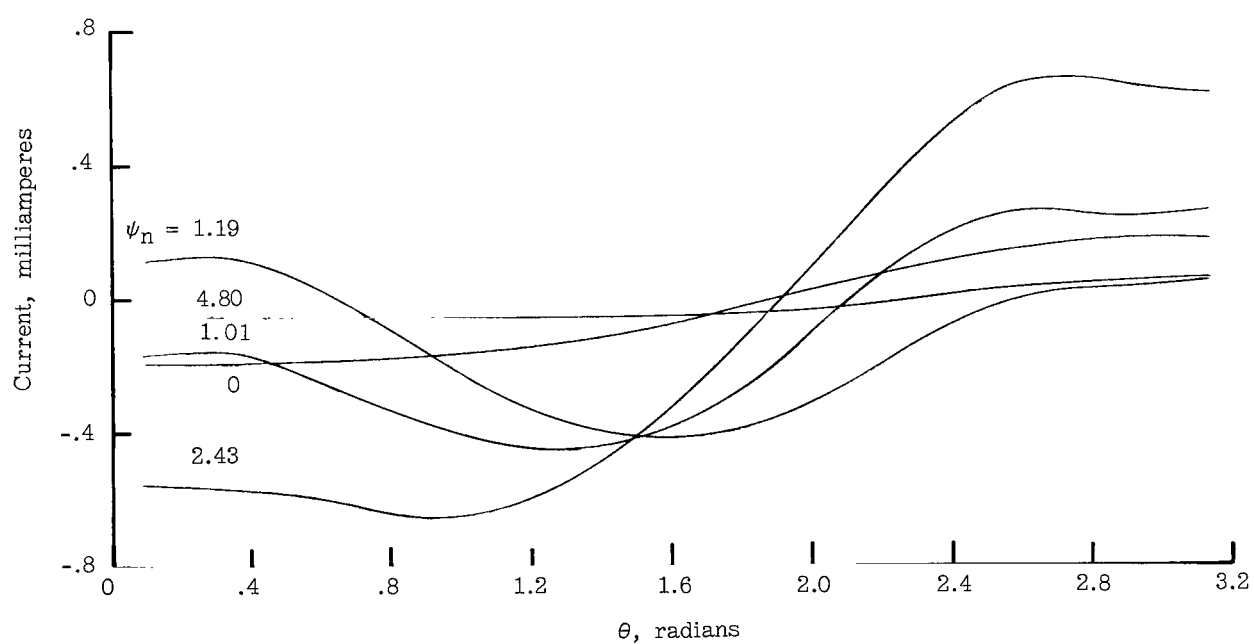


Figure 22.- Variation of induction current for Echo II for several gores without photoemission.  $\beta = 0.7$  radian.

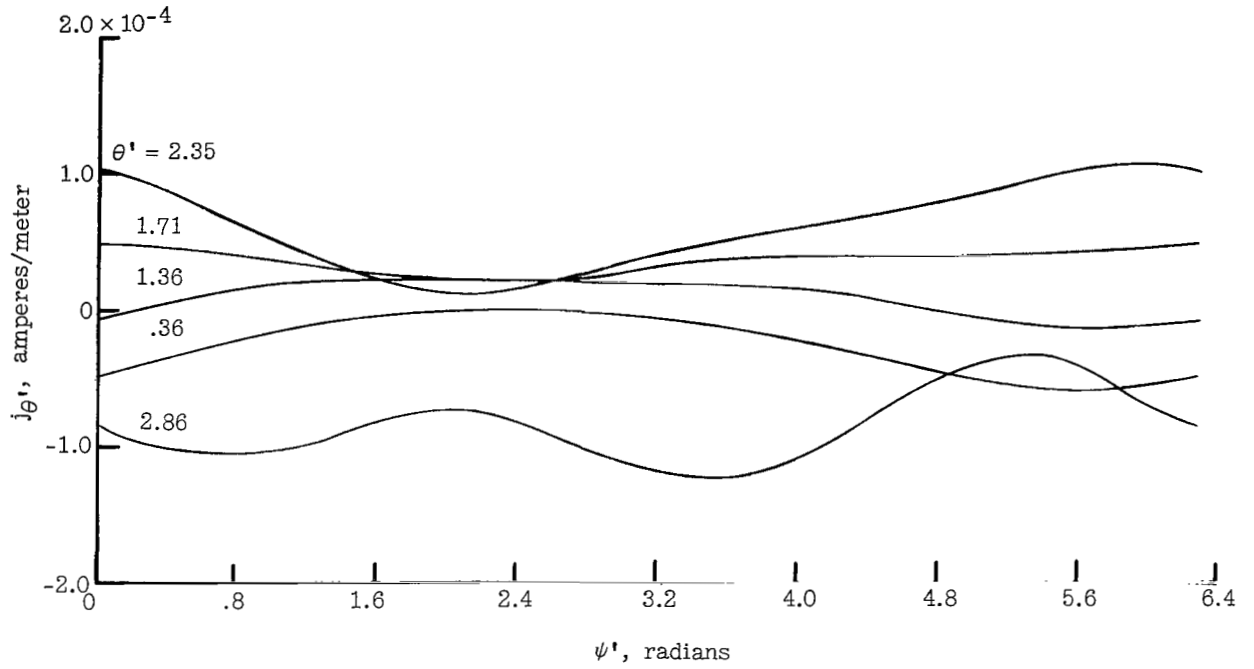


(a) Orientation I.

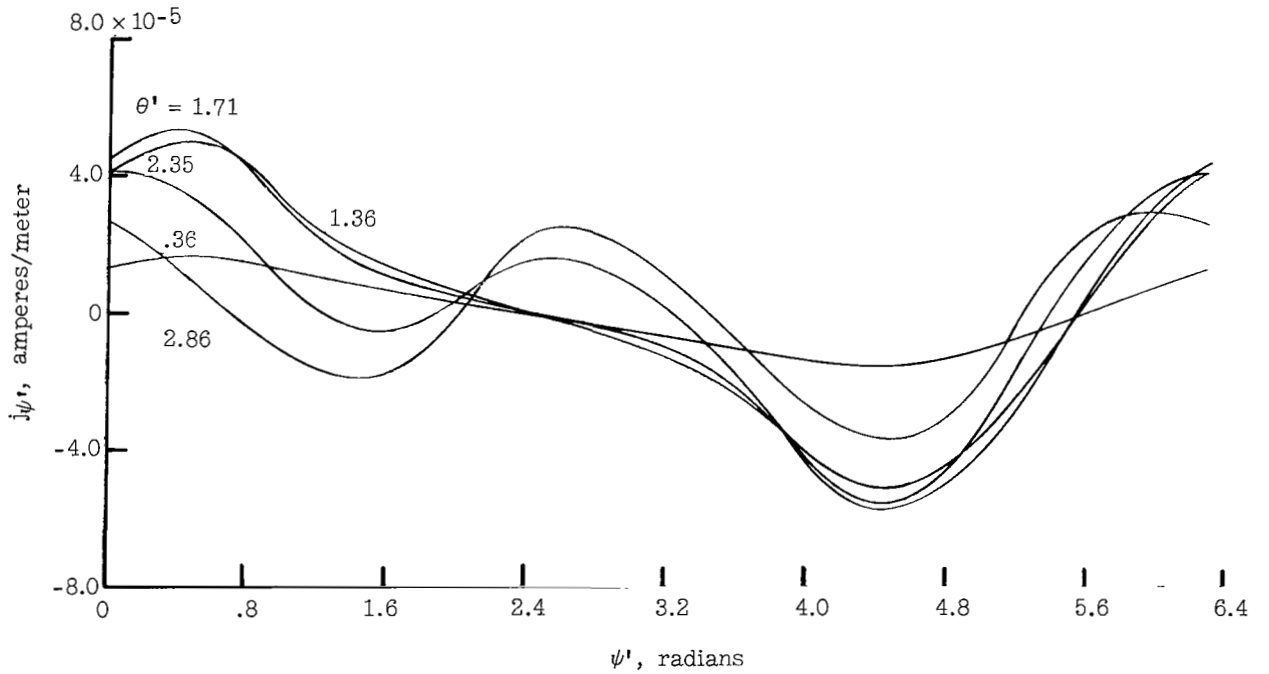


(b) Orientation II.

Figure 23.- Variation of induction current for Echo II for several gores with photoemission.  $\beta = 0.7$  radian.

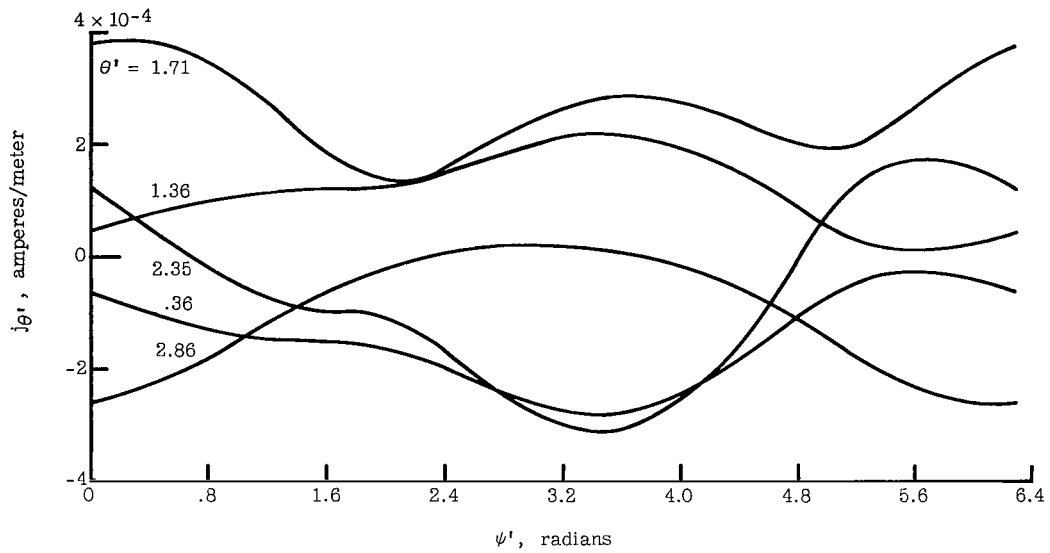


(a)  $j_{\theta'}$ .

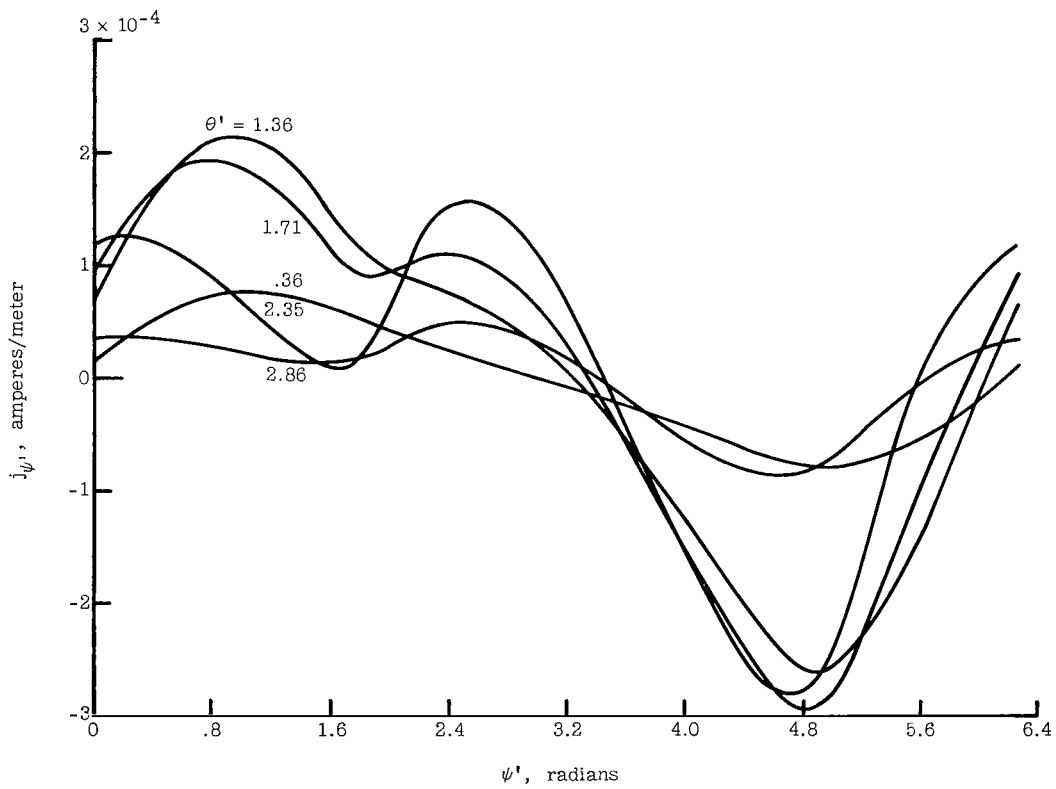


(b)  $j_{\psi'}$ .

Figure 24.- Variation of induction current density for uniformly conducting satellite without photoemission.  $\beta = 0.7$  radian.

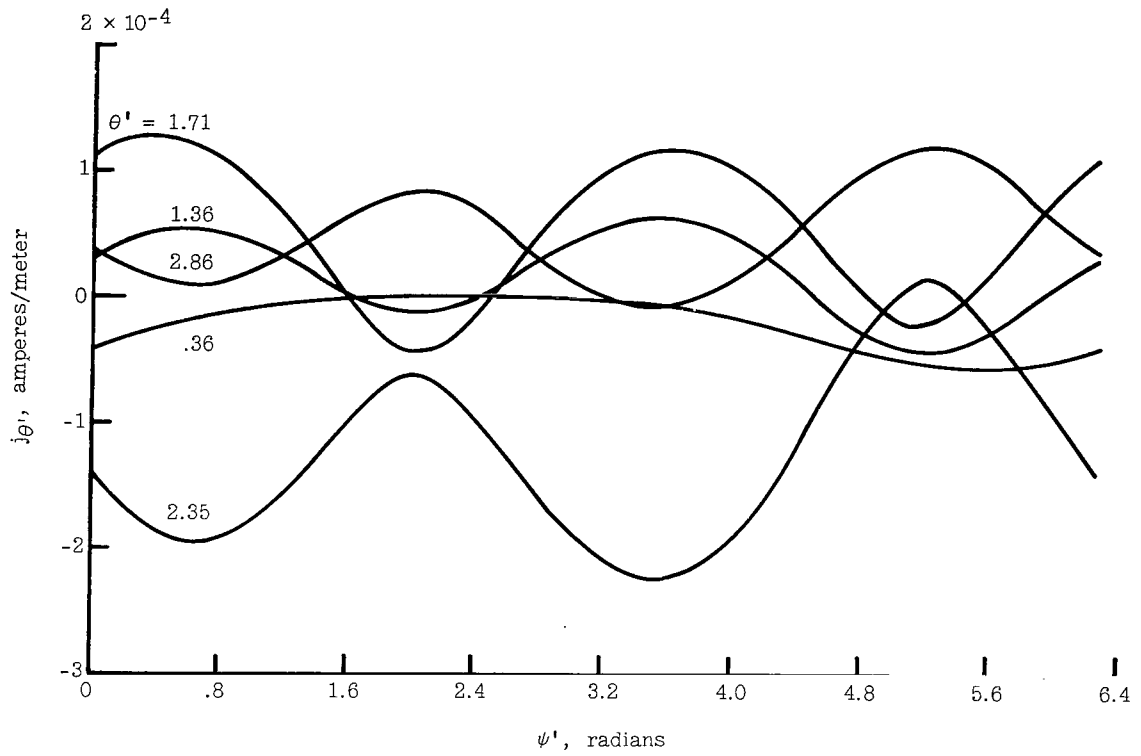


(a)  $j_{\theta'}$ .

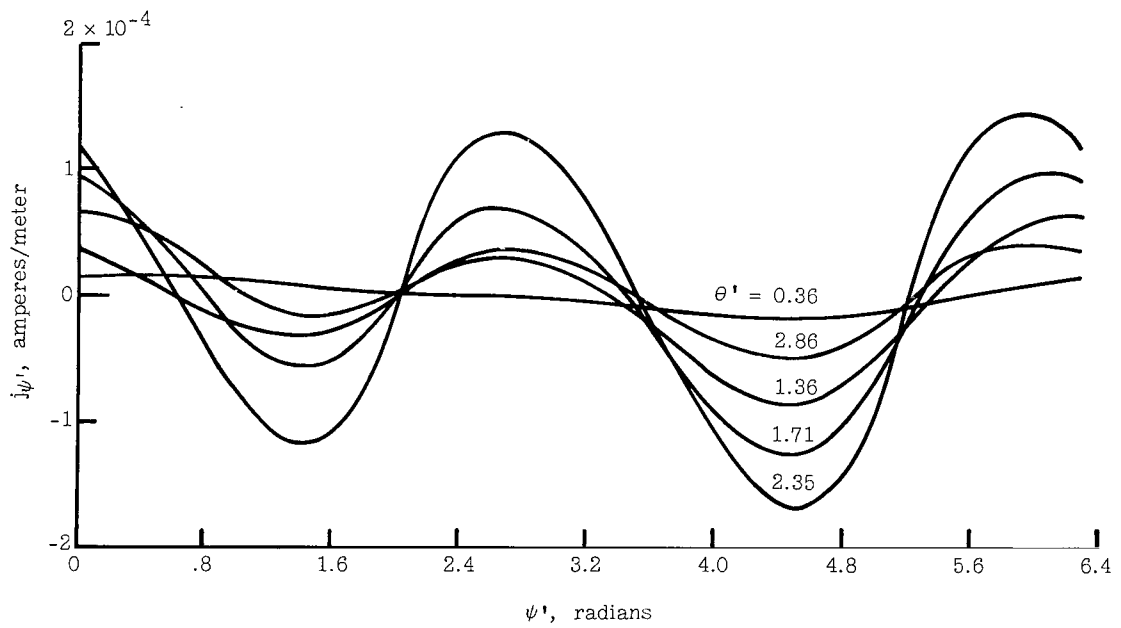


(b)  $j_{\psi'}$ .

Figure 25.- Variation of induction current density for uniformly conducting satellite with photoemission for orientation I and  $\beta = 0.7$  radian.

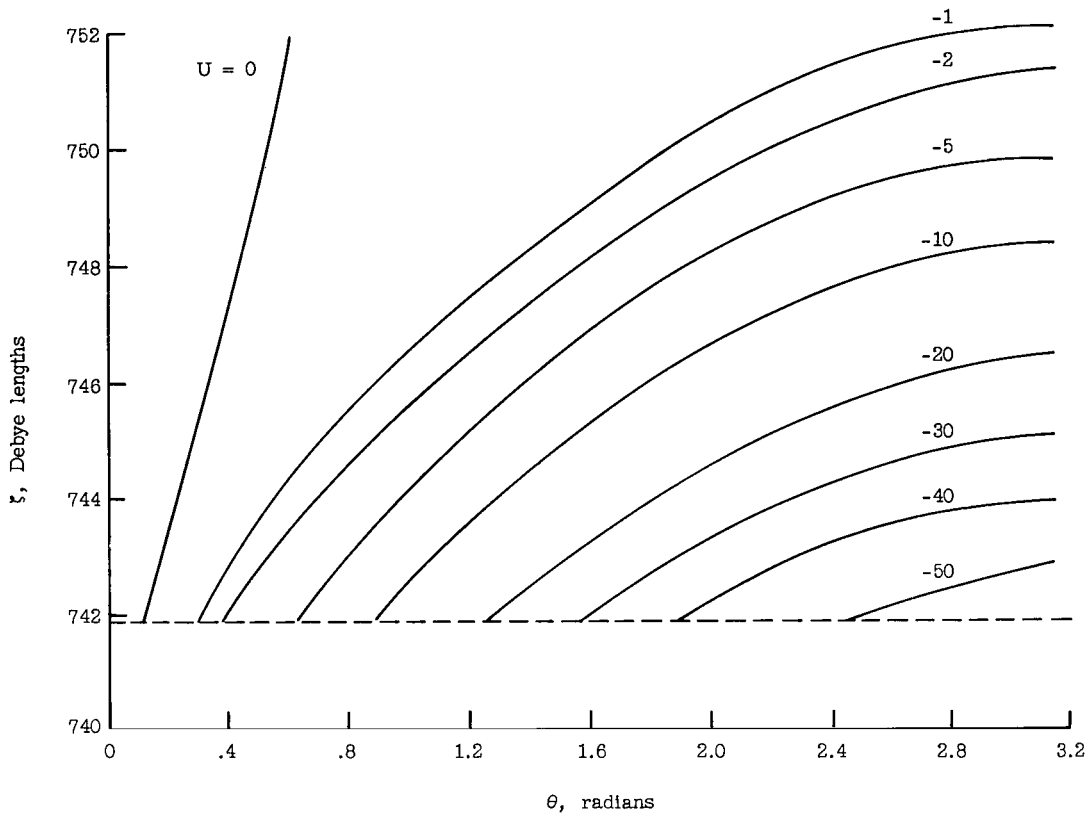


(a)  $j_{\theta'}$ .

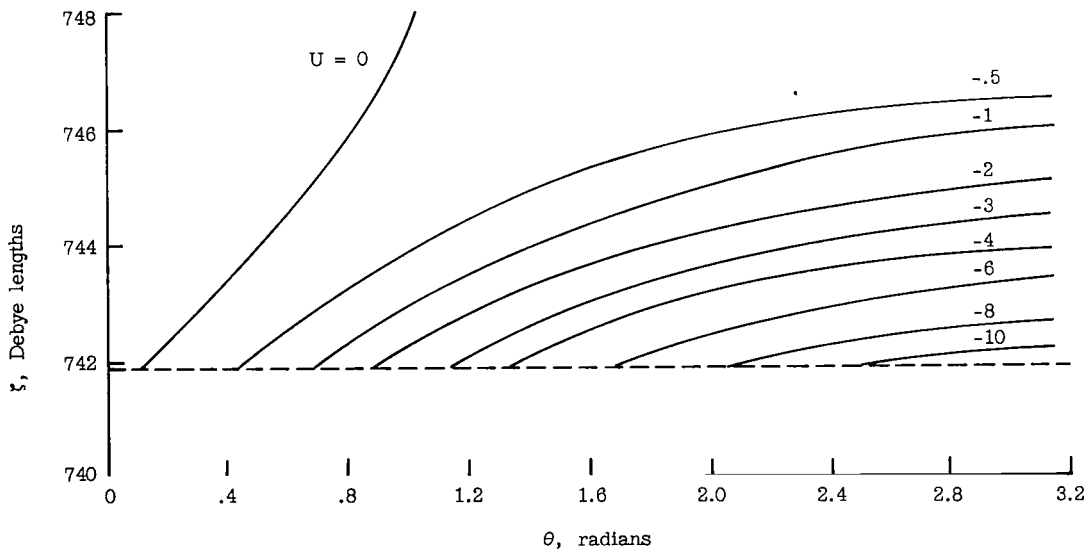


(b)  $j_{\psi'}$ .

Figure 26.- Variation of induction current density for uniformly conducting satellite with photoemission for orientation II and  $\beta = 0.7$  radian.

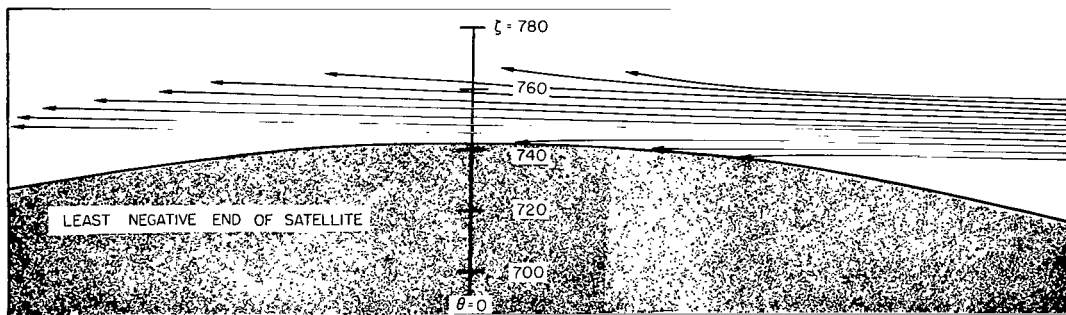


(a)  $\beta = 0.4$  radian.

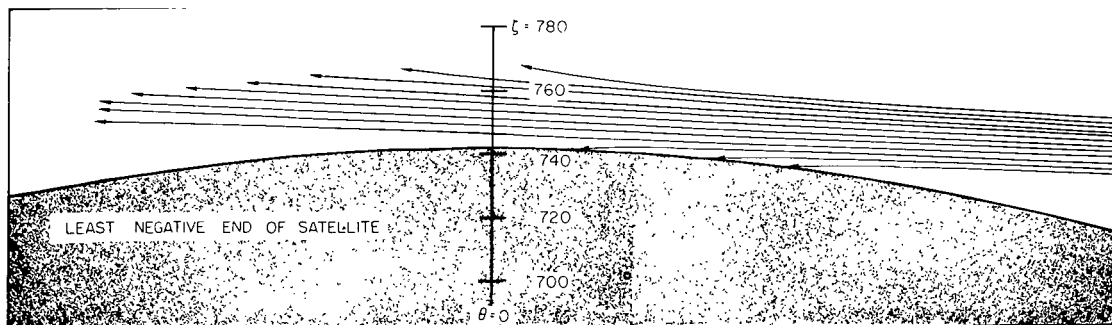


(b)  $\beta = 1.39$  radians.

Figure 27.- Potential distribution around the satellite.  $\zeta_s = 741.95$  Debye lengths.  $\left( U = \frac{e\phi}{kT} \right)$



(a)  $\beta = 0.4$  radian.



(b)  $\beta = 1.39$  radians.

Figure 28.- Ion trajectories for Echo II.  $\zeta_s = 741.95$  Debye lengths.

*"The aeronautical and space activities of the United States shall be conducted so as to contribute . . . to the expansion of human knowledge of phenomena in the atmosphere and space. The Administration shall provide for the widest practicable and appropriate dissemination of information concerning its activities and the results thereof."*

—NATIONAL AERONAUTICS AND SPACE ACT OF 1958

## NASA SCIENTIFIC AND TECHNICAL PUBLICATIONS

**TECHNICAL REPORTS:** Scientific and technical information considered important, complete, and a lasting contribution to existing knowledge.

**TECHNICAL NOTES:** Information less broad in scope but nevertheless of importance as a contribution to existing knowledge.

**TECHNICAL MEMORANDUMS:** Information receiving limited distribution because of preliminary data, security classification, or other reasons.

**CONTRACTOR REPORTS:** Technical information generated in connection with a NASA contract or grant and released under NASA auspices.

**TECHNICAL TRANSLATIONS:** Information published in a foreign language considered to merit NASA distribution in English.

**TECHNICAL REPRINTS:** Information derived from NASA activities and initially published in the form of journal articles.

**SPECIAL PUBLICATIONS:** Information derived from or of value to NASA activities but not necessarily reporting the results of individual NASA-programmed scientific efforts. Publications include conference proceedings, monographs, data compilations, handbooks, sourcebooks, and special bibliographies.

*Details on the availability of these publications may be obtained from:*

SCIENTIFIC AND TECHNICAL INFORMATION DIVISION  
NATIONAL AERONAUTICS AND SPACE ADMINISTRATION  
Washington, D.C. 20546